

University of Windsor

Scholarship at UWindor

Electronic Theses and Dissertations

Theses, Dissertations, and Major Papers

7-17-1969

Damping factors in turbine blade vibration.

Walter J. Pastorius
University of Windsor

Follow this and additional works at: <https://scholar.uwindsor.ca/etd>

Recommended Citation

Pastorius, Walter J., "Damping factors in turbine blade vibration." (1969). *Electronic Theses and Dissertations*. 6580.

<https://scholar.uwindsor.ca/etd/6580>

This online database contains the full-text of PhD dissertations and Masters' theses of University of Windsor students from 1954 forward. These documents are made available for personal study and research purposes only, in accordance with the Canadian Copyright Act and the Creative Commons license—CC BY-NC-ND (Attribution, Non-Commercial, No Derivative Works). Under this license, works must always be attributed to the copyright holder (original author), cannot be used for any commercial purposes, and may not be altered. Any other use would require the permission of the copyright holder. Students may inquire about withdrawing their dissertation and/or thesis from this database. For additional inquiries, please contact the repository administrator via email (scholarship@uwindsor.ca) or by telephone at 519-253-3000ext. 3208.

INFORMATION TO USERS

This manuscript has been reproduced from the microfilm master. UMI films the text directly from the original or copy submitted. Thus, some thesis and dissertation copies are in typewriter face, while others may be from any type of computer printer.

The quality of this reproduction is dependent upon the quality of the copy submitted. Broken or indistinct print, colored or poor quality illustrations and photographs, print bleedthrough, substandard margins, and improper alignment can adversely affect reproduction.

In the unlikely event that the author did not send UMI a complete manuscript and there are missing pages, these will be noted. Also, if unauthorized copyright material had to be removed, a note will indicate the deletion.

Oversize materials (e.g., maps, drawings, charts) are reproduced by sectioning the original, beginning at the upper left-hand corner and continuing from left to right in equal sections with small overlaps.

ProQuest Information and Learning
300 North Zeeb Road, Ann Arbor, MI 48106-1346 USA
800-521-0600

UMI[®]

DAMPING FACTORS IN
TURBINE BLADE
VIBRATION

A Thesis

Submitted to the Faculty of Graduate Studies through the
Department of Mechanical Engineering in Partial Fulfilment
of the Requirements for the Degree of
Master of Applied Science at the
University of Windsor

by

Walter J. Pastorius

Windsor, Ontario

1969

UMI Number: EC52763

UMI[®]

UMI Microform EC52763
Copyright 2007 by ProQuest Information and Learning Company.
All rights reserved. This microform edition is protected against
unauthorized copying under Title 17, United States Code.

ProQuest Information and Learning Company
789 East Eisenhower Parkway
P.O. Box 1346
Ann Arbor, MI 48106-1346

APPROVED BY:

W. North

C. Abdel-Sayed

A. Hassan

254461

ABSTRACT

In this investigation, a study is made of the three forms of turbine blade damping--root, hysteretic and aerodynamic--which may exist in the common gas turbine engine. Hysteretic and aerodynamic damping were studied in natural decay while root damping was studied under forced vibration.

A number of uniform cantilever beams were tested. Various geometries and materials were considered to determine material damping constants and to study the effects of geometry on aerodynamic damping.

The results indicate that material hysteresis damping is a function of frequency and stress distribution.

Aerodynamic damping in still air is shown to be a function of frequency, blade geometry and blade deflection shape. In the first flexural mode, aerodynamic and hysteretic damping are shown to be of the same order of magnitude.

Root damping is shown to be large at low rotational speeds but insignificant at typical design speeds.

ACKNOWLEDGEMENT

I would like to express my sincere thanks to my advisor, Dr. W. P. T. North, for his encouragement and guidance during this investigation.

The financial support of the National Research Council of Canada in the form of Grant Number A3360 and a Postgraduate Scholarship, was greatly appreciated.

In addition, I would like to express my gratitude to the Central Research Shop of the University of Windsor, Orenda Limited of Toronto and United Aircraft of Canada, Limited of Longueuil, Quebec for their assistance in the procurement and fabrication of test specimens.

TABLE OF CONTENTS

	Page
ABSTRACT.....	iii
ACKNOWLEDGEMENT.....	iv
TABLE OF CONTENTS.....	v
LIST OF FIGURES.....	vii
NOMENCLATURE.....	ix
1. INTRODUCTION.....	1
1.1 Subject of the Investigation.....	1
1.2 Importance of Damping in Turbine Blade Vibration..	1
1.3 Plan of Treatment.....	3
2. LITERATURE REVIEW.....	4
2.1 Material Hysteresis Damping.....	4
2.2 Aerodynamic Damping.....	5
2.3 Root Damping.....	6
3. OUTLINE OF THE PROBLEM STUDIED.....	7
3.1 Vibrations in Turbine Blades.....	7
3.2 Damping.....	7
3.2.1 Classical Damping Theory.....	8
3.3 Major Assumptions.....	12
3.3.1 General Assumptions.....	12
3.3.2 Blade Effect Assumptions.....	12
3.4 Geometric Configurations Studied.....	13
3.4.1 Blade Effects.....	13
3.4.2 Root Geometries Studied.....	13
3.5 Theoretical Considerations.....	14
3.5.1 Hysteretic Energy Dissipation for a Uniform Cantilever Beam.....	14

	Page
3.5.2 Aerodynamic Energy Loss	17
3.5.3 Root Damping.....	17
4. EXPERIMENTAL ARRANGEMENT AND PROCEDURE.....	19
4.1 Blade Effects.....	19
4.2 Root Effects.....	19
5. RESULTS AND DISCUSSION OF THE ANALYSIS.....	20
5.1 Blade Effects.....	20
5.1.1 Hysteretic Damping.....	20
5.1.2 Aerodynamic Damping.....	22
5.2 Root Effects.....	23
5.3 Estimate of Experimental Errors.....	24
6. RECOMMENDATIONS.....	29
6.1 Suggestions for Experimental Improvement.....	29
6.2 Suggestions for Futher Work.....	29
7. CONCLUSIONS.....	30
8. BIBLIOGRAPHY.....	31
APPENDIX.....	61
A. MATERIAL AND GEOMETRIC PROPERTIES OF THE BEAMS TESTED...	61
B. VIBRATION MONITORING DEVICES USED.....	63
C. BLADE EFFECTS TEST EQUIPMENT.....	65
D. FORCED VIBRATION SYSTEM.....	71
E. ROOT EFFECT TEST EQUIPMENT.....	75
F. CALIBRATION OF STRAIN GAGE OUTPUT AGAINST TIP DEFLECTION	76
G. EFFECTS OF TAPER ON HYSPERETIC DAMPING.....	78
H. AERODYNAMIC ENERGY LOSS IN MOVING AIR	84
I. COMMERCIAL EQUIPMENT USED.....	86
VITA.....	87

LIST OF FIGURES

<u>Figure</u>		<u>Page</u>
1	Specific Damping Capacity against Amplitude of Reversed Stress (20 cpm) (from ref. 17).....	35
2	Typical Nodal Patterns for a Compressor Blade.....	36
3	Typical Nodal Patterns for a Uniform Cantilever.....	36
4	Beam Geometries Studied.....	37
5	Root Sections Studied.....	38
6	Beam No. 1- Natural Decay Test- Tip Deflection against Cycles.....	39
7	Beam No. 2- Natural Decay Test- Tip Deflection against Cycles.....	40
8	Beam No. 3- Natural Decay Test- Tip Deflection against Cycles.....	41
9	Beam No. 4- Natural Decay Test- Tip Deflection against Cycles.....	42
10	Beam No. 5- Natural Decay Test- Tip Deflection against Cycles.....	43
11	Beam No. 6- Natural Decay Test- Tip Deflection against Cycles.....	44
12	Beam No. 7- Natural Decay Test- Tip Deflection against Cycles.....	45
13	Beam No. 8- Natural Decay Test- Tip Deflection against Cycles.....	46
14	Frequency Dependence of Material Damping Constant J for 6061-T6 Aluminum.....	47
15	Frequency Dependence of Material Damping Exponent n for 6061-T6 Aluminum.....	48
16	Beam No. 1. Energy Loss against Tip Deflection.....	49
17	Beam No. 2. Energy Loss against Tip Deflection.....	50
18	Beam No. 3. Energy Loss against Tip Deflection.....	51
19	Beam No. 4. Energy Loss against Tip Deflection.....	52
20	Beam No. 5. Energy Loss against Tip Deflection.....	53

<u>Figure</u>		<u>Page</u>
21	Beam No. 6- Energy Loss against Tip Deflection.....	54
22	Beam No. 7- Energy Loss against Tip Deflection.....	55
23	Beam No. 8- Energy Loss against Tip Deflection.....	56
24	Aerodynamic Energy Loss against Tip Deflection.....	57
25	Aerodynamic/Hysteretic Energy Loss against Tip Deflection.....	58
26	Root Damping against Equivalent Rotor Speed.....	59
27	Non- Dimensional Beam Displacement Profile Beam No.4.....	60
28	Hysteretic Damping Capacity against Stress.....	62
29	Shaker Table.....	64
30	Portion of a typical Curve from the Light-Beam Recorder.....	66
31	Block Diagram of Natural Decay Test Apparatus.....	67
32	Natural Decay Test Arrangement.....	68
33	Natural Decay Test Rig.....	69
34	Vacuum Chamber.....	70
35	Block Diagram of Forced Vibration Excitation Apparatus.....	72
36	General Laboratory Arrangement Forced Vibration Tests.....	73
37	Typical Level Recorder Output - Frequency against Amplitude.....	74
38	Typical Calibration of Strain Gage Output against Tip Deflection.....	77
39	Taper Nomenclature.....	79
40	Effect of Depth Taper on Beam Displacement Shape (First Flexural Mode).....	81
41	Effect of Width Taper on Beam Displacement Shape (First Flexural Mode).....	82
42	Effect of Taper on Hysteretic Energy Dissipation against Tip Deflection.....	83

NOMENCLATURE

A	cross-sectional area
A_0	cross-sectional area at blade base
A_t	cross-sectional area at blade tip
b	beam width
c	chord
D	specific damping capacity
d	damping factor
Δ	amplitude (single peak)
Δ_{pk}	tip amplitude (single peak)
Δ_{st}	static deflection
δ	logarithmic decrement
δ_a	logarithmic decrement due to air only
δ_t	taper coefficient
E	Young's modulus of elasticity
e	base of natural logarithms
f	frequency
f_R	resonant frequency
g	acceleration due to gravity
h	beam thickness
I	moment of inertia
I_0	moment of inertia at blade base
J	material damping constant
l	beam length
M	bending moment
m	mass
n	material damping exponent

p	period
ρ_a	density of air
ρ_m	density of blade material
r	frequency ratio
∇	stress
t	time
U	strain energy
ΔU	loss in strain energy over one cycle
v	air velocity relative to the blade
v	blade velocity
ω	circular frequency

1. INTRODUCTION

1.1 SUBJECT OF THE INVESTIGATION

The purpose of this investigation was to determine the relative importance of root, aerodynamic and material hysteresis damping as applied to the blades of a gas turbine engine, and the parameters involved in these quantities.

1.2 IMPORTANCE OF DAMPING IN TURBINE BLADE VIBRATION

Vibration is a major problem in the turbine engine since it leads to high fluctuating stresses which can cause fatigue failure of a blade in a very short time. Operating experience with gas turbines in military aircraft shows that rotor blades in axial compressors are the most unreliable single item (1). Blade vibration generally is caused by some forcing function within the engine itself which has a frequency near a natural resonant frequency of a blade, or some harmonic of this natural frequency. The excitation may be an aerodynamic fluctuation superimposed on the nominal gas bending loads on the blades (2), (3), (4) or may be a mechanical vibration from some source such as a gearbox.

Early gas turbine engines could operate efficiently only at one fixed design speed. Hence, if blade failures occurred due to vibration, blade geometry could be altered to change the blade resonance frequencies away from all excitation frequencies.

However, recent trends to higher efficiency engines, coupled with the demands of the aircraft industry for reduced weight, have caused further vibration problems. The advent of the variable nozzle guide

vane engine, which can operate at high efficiency over a wide range of rotor speeds, creates the problem of a wide range of forcing function frequency possibilities as rotor speed is varied. Also, one of the most obvious ways to increase overall engine efficiency is to increase the turbine inlet temperature. This increases actual blade temperature which reduces fatigue strength, making blade vibration more critical.

Thus, other forms of preventing or reducing blade resonance have been sought. The lacing together of several blades either by wires or rods is popular since it may be applied to an engine already in production. However, the method has several serious disadvantages: lacing disturbs the air flow which reduces efficiency; a stress concentration is introduced in the blade where the lacing is attached; and it may solve a vibration problem in one mode only to create a serious problem in another complex mode due to the extra boundary condition on the blade (5). Hence, the use of blade lacing is mainly an emergency stop-gap measure until design improvements can be made.

Tip shrouding has been used successfully in many designs. However, the shroud increases centrifugal forces on the blade and hence tends to increase blade creep. Also, tip shrouding generally increases blade fabrication costs.

The question of damping, or dissipation of vibratory energy, is important. Three forms of damping may exist in the common turbine engine: A) material hysteresis damping; B) aerodynamic damping; and C) root damping.

A. MATERIAL HYSTERESIS DAMPING This exists due to a slight hysteresis or anelastic phenomenon between stress and strain. This

energy is dissipated through heat in the blade.

B. AERODYNAMIC DAMPING This results from the dissipation of energy of vibration to the atmosphere surrounding the blade due to both the formation of vortices along the blade edge and work done on the air by the blade during vibration.

C. ROOT DAMPING This will dissipate energy at the blade root due to sliding friction if any relative motion exists between the blade root and the disk fixture.

1.3 PLAN OF TREATMENT

The analysis was split into two segments: blade effects; and root effects. Both aerodynamic and hysteretic damping were included in the former while root damping made up the latter. Blade effects were studied by tests in natural decay. Aerodynamic damping was reduced to a negligible amount by placing specimens in a vacuum chamber. Specimens were then tested under atmospheric conditions. The increase in damping in the second case was attributed to aerodynamic effects.

Root effects were studied by forced vibration tests. Two actual cases were considered--that of a fir tree root and that of a dovetail root.

2. LITERATURE REVIEW

2.1 MATERIAL HYSTERESIS DAMPING

The nature of internal hysteresis in solids was investigated in the period of 1926-28 by Kimball (6), (7), (8), (9). He initially proposed that energy loss was proportional to stress squared, a case similar to classical viscous friction. His tests were carried out on rotating rods at frequencies generally below 50 cps. He later found that damping was proportional to some power of the stress, not necessarily two, and that an upper stress limit existed near the yield stress where damping increased rapidly. In all cases, Kimball found no dependence of damping on frequency below 50 cps.

In 1932, S. F. Dorey found that hysteresis energy loss was proportional to stress cubed (below some critical stress value) for typical crankshaft steels (10). In 1946, Robertson and Yorgiadis also found a third order dependence of damping on stress. They also found damping to be independent of frequency up to 100 cps (11). Marin and Stulen found similar results in 1947 (12).

In 1950, B. J. Lazan began a series of tests to study damping problems (13), (14), (15), (16). He found that damping was proportional to stress raised to some power. This power varied from two to thirty. After studying many materials in tests on rotating beams (14) and in bending specimens (15), he suggested several general conclusions. At room temperature, and for constant stress, damping was found to settle out after about 500 cycles and to decrease very slightly with cycles until failure occurred. At high temperatures, large changes in damping occurred at large numbers of cycles. The dynamic modulus of elasticity

was found to be within 5% of the static value for low stress levels, with very slight dependance on cycles. He found the critical limit for damping as a function of stress to a power to be essentially independant of cycles and to lie at approximately 80% of the material endurance limit. If this value, the sensitivity limit, was exceeded, damping increased rapidly (figure 1). The majority of this work was done at 20 cpm, giving no information of frequency dependance of damping. A tabulation of many of Lazan's results is given by Marin (17).

An interesting electrical analogy for hysteretic damping is given by Soroka (18) but no experimental correlation is given.

2.2 AERODYNAMIC DAMPING

The steady, nominal gas bending loads on a blade have been studied by many investigators under several methods, such as Kavanagh and Serovy (19). Superimposed on these loads are fluctuating aerodynamic loads due to upstream interruptions of flow or flow instability (2), (3), (4). These fluctuating forces generally act as exciting forces.

Depending on the flow properties, angle of incidence and blade geometry, this flow may cause the blade to vibrate, due to its aerodynamic shape, or may actually do negative work on the blade, i.e. damp blade vibrations.

Several investigators have studied aerodynamic damping on flat cantilevers. Baker, Woolam and Young (20), suggested that two forms of damping exist, one proportional to velocity, the other proportional to velocity squared. Based on natural decay tests, they suggest that air damping is significant at all amplitudes, with damping dominantly proportional to velocity squared at high amplitude and proportional to

velocity at small amplitude. They do not compare the results to theory,⁶ nor do they attempt to determine the transition point between the two types of damping.

McWithey (21), tested 20" x 1" x $\frac{1}{4}$ " beams of 4130 stainless steel up to maximum tip amplitudes of 0.438 inches in natural decay. He found aerodynamic damping to be negligible at small amplitudes but significant at large amplitudes.

Hanson, Meyer and Manson (22) have found good experimental verification of a theoretical solution to aerodynamic damping theory. The theory used included vortex losses along the blade edges as well as propulsive losses along the blade faces.

2.3 ROOT DAMPING

The problem of root damping is affected by contact stresses in the root fixture. These stresses have been analyzed statically for several types of fixtures by Durelli, Dally and Riley (23).

A theoretical analysis of root damping has been done by Goodman and Klump (24). A controlled experiment verified the results and a correlation with actual engine results was suggested, based on uniform pressure theory.

Goatham and Smailes (25) suggest that the use of pin-connected roots may be effective in reducing vibratory stresses. Experimental results for pin-connected roots (22) verify this conclusion.

An evaluation of single and double ball roots has been done experimentally by Manson (26). His results show that root damping may be effective at low rotational speeds or under large vibratory forcing functions.

3 OUTLINE OF THE PROBLEM STUDIED

3.1 VIBRATIONS IN TURBINE BLADES

A great number of factors affect vibrations in turbine blades. Temperature variation from ambient to operating conditions with the associated changes in material properties can change blade natural frequencies up to 20% (27). The stiffening effect of centrifugal force can significantly alter blade resonant frequencies with small changes in engine rotational speed. Natural frequencies can also be altered by deposits on blades such as from salt water ingestion and soot in the turbine section, as well as by blade erosion and corrosion.

Aerodynamic effects change with gas temperature and pressure which can vary considerably through an engine from inlet conditions to combustor outlet conditions. Inlet blockages due to leaves or ingested birds can cause very large fluctuations of aerodynamic conditions.

Material hysteresis damping constants may vary greatly with temperature and stress, particularly if the material hysteresis sensitivity limit is exceeded (figure 1).

Root contact stresses and hence root damping are a function of centrifugal force, fretting, temperature, lubrication and root machining tolerances.

The complex geometry of common blade profiles creates a very difficult stress analysis problem. A common blade may be tapered in both thickness and in chord, twisted, and curved. Typical nodal patterns for a compressor blade are shown in figure 2. Comparison of these nodal patterns with those of a uniform cantilever beam (figure 3) shows the complex nature of dynamic analysis of turbine blades.

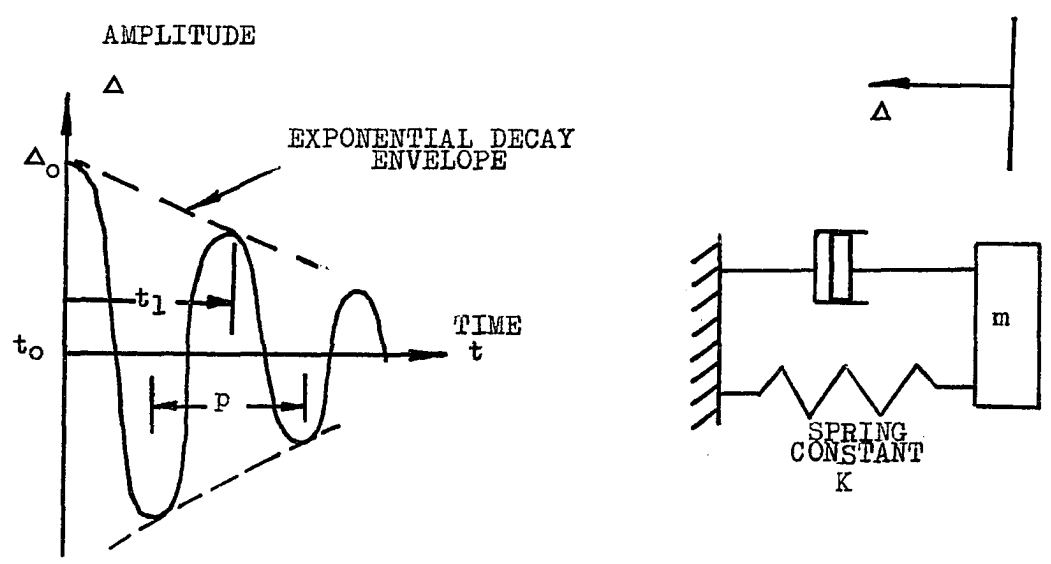
3.2 DAMPING

Damping serves to dissipate energy of vibration and to limit vibratory amplitude. Theoretically, if energy were fed into a system with zero damping capacity at a resonant frequency of that system, the amplitude of vibration would become infinite. In actual fact, damping of one or more forms exists in every physical system.

The two classical forms of damping - viscous and coulombic - have been well documented. Viscous damping is proportional to velocity squared and coulombic damping is proportional to velocity. In most engineering work, however, much more complex, non-linear forms of damping are present.

Whenever it is desired to decrease vibratory amplitudes, an obvious solution is to increase damping. If a sufficiently large amount of damping can be built into a system, even a substantial excitation force will not cause severe vibrations.

3.2.1 Classical Damping Theory
Natural Decay



The classical natural decay curve, as shown above, may be written (28)

$$\Delta = Ae^{-kt} \cos \omega t \quad \text{and} \quad p = \frac{2\pi}{\omega}$$

Substituting the initial condition $\Delta = \Delta_0$ at $t = t_0 = 0$

$$A = \Delta_0$$

One cycle later, at $t = t_1 = \frac{2\pi}{\omega}$

$$\Delta|_{t_1} = \Delta_0 \exp\left(-\frac{2\pi k}{\omega}\right)$$

Then the logarithmic decrement, by definition,

$$\delta = \ln \left[\frac{\Delta|_{t_0}}{\Delta|_{t_1}} \right]$$

$$\delta = \frac{2\pi k}{\omega}$$

or the constant

$$k = \frac{\delta \omega}{2\pi}$$

For the simple spring-mass-dashpot system, net potential energy at t_0 may be written

$$U(t_0) = \frac{1}{2} K \Delta_0^2$$

where K represents the spring constant. Net potential energy at $t_1 = \frac{2\pi}{\omega}$

$$U(t_1) = \frac{1}{2} K \Delta_0^2 \exp(-2\delta)$$

Then energy loss in the one cycle

$$\begin{aligned} \Delta U &= U(t_0) - U(t_1) \\ &= \frac{1}{2} K \Delta_0^2 (1 - \exp(-2\delta)) \end{aligned}$$

For small δ , $e^{-2\delta} \ll 1$ and the total energy at any point in the cycle may be written

$$U = U(t_0) \approx U(t_1)$$

Then

$$\begin{aligned} \frac{\Delta U}{U} &= \frac{\frac{1}{2} K \Delta_0^2 (1 - \exp(-2\delta))}{\frac{1}{2} K \Delta_0^2} \\ &= 1 - \exp(-2\delta) \end{aligned}$$

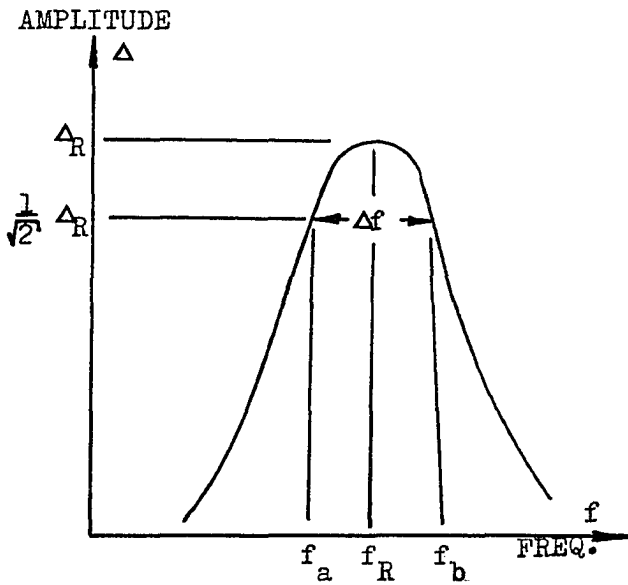
Applying a Maclaurin expansion

$$\frac{\Delta U}{U} = 1 - 1 + 2\delta - \frac{(2\delta)^2}{2!} + \dots$$

which, neglecting terms in δ^2 reduces to

$$\delta = \frac{\Delta U}{2U} \quad \text{-----} \quad (A)$$

Hence, the logarithmic decrement is approximately one half the ratio of net energy loss per cycle to total energy in the cycle.



It is also desirable to relate the log decrement to the resonance curve bandwidth. For a simple system, the shape of the resonance curve is given by (28)

$$\frac{\Delta}{\Delta_{st}} = \frac{1}{\sqrt{(1-r^2)^2 + r^2 d^2}}$$

where Δ_{st} = static deflection under systems own weight

Δ = amplitude at frequency f

$r = f/f_r$ frequency ratio where f_r is the resonant frequency

d = damping factor

At resonance, $r=1$ and

$$\frac{\Delta_R}{\Delta_{st}} = \frac{1}{d}$$

At the points where the amplitude is reduced to $\frac{1}{\sqrt{2}}$ of the resonant amplitude

$$\Delta = \frac{\sqrt{2}}{2} \Delta_R = \frac{\sqrt{2}}{2} \frac{\Delta_{st}}{d}$$

Substituting in the frequency equation

$$\frac{\sqrt{2}}{2} \frac{1}{d} = \frac{1}{\sqrt{(1-r^2)^2 + r^2 d^2}}$$

or

$$\frac{1}{2d^2} = \frac{1}{(1-r^2)^2 + r^2 d^2}$$

Solving for the frequency ratio

$$r^2 = 1 - \frac{d^2}{2} \pm d \sqrt{\frac{d^2}{4} + 1}$$

Neglecting terms in d^2 since d is small.

$$\begin{aligned} r^2 &= 1 \pm d \\ \frac{f}{f_R} = r &= 1 \pm \frac{d}{2} - \frac{d^2}{4} + \dots \\ &\approx 1 \pm \frac{d}{2} \end{aligned}$$

which gives the frequencies at the points where the amplitude is reduced to $\frac{1}{\sqrt{2}}$ of the resonant amplitude as

$$\begin{aligned} f_a &= f_R \left(1 - \frac{d}{2}\right) \\ f_b &= f_R \left(1 + \frac{d}{2}\right) \end{aligned}$$

Then $\Delta f = df_R$

or

$$d = \frac{\Delta f}{f_R}$$

In natural decay (27), for small damping

$$\delta = \frac{\pi d}{\sqrt{1 - \left(\frac{d}{2}\right)^2}} \approx \pi d$$

Hence, the log decrement in terms of the resonance bandwidth is given by

$$\delta = \frac{\pi \Delta f}{f_R} \quad \text{-----} \quad (B)$$

Although the above analysis applies strictly only to classical cases, it is considered suitably accurate for this analysis.

3.3 MAJOR ASSUMPTIONS

3.3.1 General Assumptions

The following assumptions were made:

1) The jigs used have negligible effects on vibration and damping.

2) Damping is small and is a continuous function of amplitude or stress.

3) Effects of shear deflection and rotary inertia are small.

4) The dynamic deflection curve of a uniform cantilever beam is similar to the static beam deflection curve when the beam is subjected to a uniform load.

5) The uniform cantilever beams vibrate in a pure first flexural mode.

6) The dynamic modulus of elasticity is essentially the same as the static modulus.

3.3.2 Blade Effect Assumptions

The following assumptions were made for the blade effect tests :

1) No aerodynamic damping exists at room temperature and a pressure of less than one psia.

2) Energy dissipation in the strain gage used is negligible.

3) Hysteretic damping is independent of cycles (stress history) in the range of cycles tested.

4) The hysteretic damping stress sensitivity limit (figure 1) was not exceeded at any time.

5) Blade temperature rise due to energy dissipated internally as heat is small.

3.4.1 Blade Effects

Due to the complex geometric and vibrational configurations of common blades (figure 2), it was decided to analyze blade effects using uniform untwisted cantilevers. The term "beam" is used to indicate a uniform cantilever as opposed to an actual turbine blade. The beams selected are given in figure 4. Relatively large beams were chosen to insure significantly large aerodynamic damping at room temperature and pressure. Stress distributions encountered should be in the range of those experienced in actual blades. Several sizes were used to determine if any correlation of aerodynamic damping to size could be found. Several materials were tested for material hysteresis analysis. The three beams of 6061-T6 aluminum (beams 1,2, and 3) were selected to compare material hysteresis damping constants at various frequencies. The frequencies selected were concurrent with those studied by Baker, Woolam, and Young (20).

3.4.2 Root Geometries Studied

Two root geometries were available for study - a fir tree root and a dovetail root. Both are shown in figure 5.

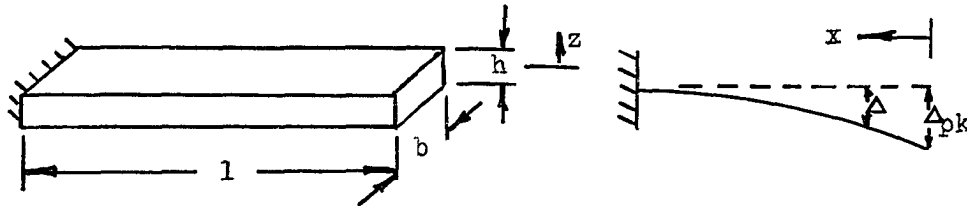
The fir tree root, from a turbine section, had three lobes on each side. The blade was made of cast Inco 713c and the disk of PWA 1003.

The dovetail root was from a compressor. The blade was made of AMS 5616.

3.5 THEORETICAL CONSIDERATIONS

3.5.1 Hysteretic Energy Dissipation for a Uniform Cantilever Beam

Consider a cantilever beam vibrating in the first flexural mode. The deflected shape of the beam is assumed similar to the beam static deflection curve under a uniform load.



The deflection curve is given by the well known formula

$$\Delta = k(x^4 - 4l^3x + 3l^4)$$

where k is a scaling constant required for deflection profile similarity. The maximum, or tip deflection is given by

$$\Delta_{pk} = 3kl^4$$

Then, the non-dimensional deflection is

$$\frac{\Delta}{\Delta_{pk}} = \frac{x^4 - 4l^3x + 3l^4}{3l^4}$$

The bending moment at any section is given by

$$\frac{M}{EI} = \frac{\frac{d^2\Delta}{dx^2}}{\left[1 + \left(\frac{d\Delta}{dx}\right)^2\right]^{3/2}}$$

which, for small strain theory, reduces to

$$\frac{M}{EI} = \frac{d^2\Delta}{dx^2}$$

Differentiating and introducing Δ_{pk} gives

$$\frac{M}{EI} = \frac{4x^2 \Delta_{pk}}{l^4} \quad \text{-----} \quad (c)$$

For bending, the stress at any point is given by

$$\sigma = \frac{Mz}{I} \quad \left(-\frac{h}{2} \leq z \leq \frac{h}{2}\right)$$

Substituting (C)

$$\sigma = \frac{4x^2 \Delta_{pk} Ez}{l^4}$$

The net internal energy dissipation for a given tip displacement may be found by integrating the specific damping capacity over the entire beam. The specific damping capacity can be written (17)

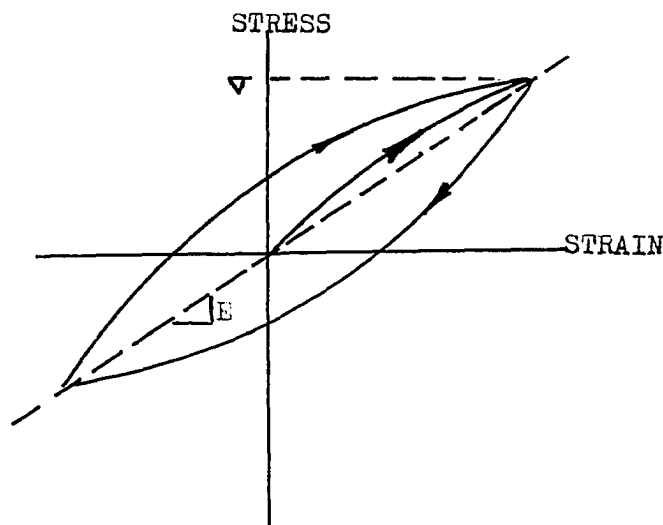
$$D = J\sigma^n \quad (\text{in.-lbs./cu. in./cycle})$$

where σ represents the maximum or peak stress at a point during a cycle and J and n are constants independent of stress. Then hysteretic energy loss per cycle for the beam is given by

$$D = 2Jb \int_{z=0}^{h/2} \int_{x=0}^1 \left[\frac{4x^2 \Delta_{pk} Ez}{l^4} \right]^n dx dz$$

(assuming symmetry of the stress distribution about $z=0$ and that energy dissipation is the same for tension as for compression.)

A typical hysteresis loop is shown below.



Evaluation of the integral yields the energy loss per cycle in the first flexural resonance as

$$D = \frac{2^n J_b E^n h^{n+1} l^{1-2n} \Delta_{pk}^n}{(n+1)(2n+1)}$$

or

$$D = \frac{J_b h l}{(n+1)(2n+1)} \left[\frac{2Eh}{l^2} \Delta_{pk} \right]^n \quad (D)$$

It is required to relate the above equation for internal energy dissipation to the beam energy loss per cycle in natural decay.

Neglecting shear, the maximum strain energy in the beam is given by

$$U = \int_0^l \frac{M}{EI} \frac{M}{2} dx$$

Substituting (C)

$$U = \int_0^l \frac{16x^4 \Delta_{pk}^2 EI}{21^8} dx$$

$$= \frac{8 \Delta_{pk}^2 EI}{5 l^3}$$

but

$$I = \frac{1}{12} b h^3$$

$$U = \frac{2Ebh^3}{15l^3} \Delta_{pk}^2$$

Then energy loss per cycle

$$\frac{dU}{d(\text{cycle})} = \frac{4Ebh^3}{15l^3} \Delta_{pk} \frac{d\Delta_{pk}}{d(\text{cycle})} \quad (E)$$

Equating (D) and (E)

$$\Delta_{pk}^{1-n} \frac{d\Delta_{pk}}{d(\text{cycle})} = \frac{15 J l^4}{4 (n+1)(2n+1) E h^2} \left[\frac{2Eh}{l^2} \right]^n \quad (F)$$

Using equation (F), material damping constants can be calculated from experimental results. Substitution of two pairs of values for Δ_{pk} and $\frac{d\Delta_{pk}}{d(\text{cycle})}$ yields two equations for J and n which may be solved to separate J and n.

3.5.2. Aerodynamic Energy Dissipation

In still air, aerodynamic energy dissipation may occur in two forms. Energy is dissipated in the creation of vortices at the tip and edges of the blade as well as by work done propulsively on the blade faces.

Total energy loss per cycle may be calculated from decay curves in still air as loss in strain energy per cycle from equation (E).

$$\frac{dU}{d(\text{cycle})} = \frac{4}{15} \frac{Ebh^3}{l^3} \Delta_{pk} \frac{d\Delta_{pk}}{d(\text{cycle})}$$

At a given value Δ_{pk} , the hysteretic energy loss per cycle, calculated from equation (E) for decay curves in the vacuum, may be subtracted from the total energy loss per cycle to yield aerodynamic energy loss per cycle.

In the experimental range tested, aerodynamic damping may be represented as being proportional to $(\Delta_{pk})^\alpha$ where " α " represents an apparent aerodynamic energy loss exponent. The value of " α " for a given beam may be found by the slope of a log-log plot of Δ_{pk} against aerodynamic energy loss per cycle.

3.5.3 Root Damping

Due to the highly complex nature of root damping, no theoretical solution was attempted. A large number of variables are involved in the problem. Contact areas must be defined as well as contact stresses. Contact area is a function of root and fixture deflection under centrifugal, gas bending and vibratory loads as well as geometric

variations within machining tolerances. Contact area is particularly difficult to define in the case of multiple fixtures ie. double ball or fir tree. Contact stress is similarly complicated. Also, the coefficient of friction is, in most cases, a function of cyclic history (24), and a distinction must be made between static and dynamic friction.

4 Experimental Arrangements And Procedure

4.1 BLADE EFFECTS

Since energy dissipation per cycle is small, natural decay tests were selected to determine damping properties. Energy dissipation was measured in terms of loss of strain energy per cycle.

Metal foil strain gages were mounted axially near the base of each beam and connected to the carrier-amplifier light-beam recorder system. Strain output against tip deflection was then calibrated (Appendix F) for the beam in the first flexural mode. Beams were run at the first flexural frequency for several minutes on the shaker table (Appendix D) to remove any material hysteresis virgin material effects.

The accelerometer on the tip of the beam was removed and the beam was clamped to the vacuum chamber base plate. The chamber cover was put in position and sealed with vacuum grease. If desired, pressure in the chamber was reduced by a vacuum pump. Pressure was monitored using a vacuum gauge.

An A.C. solenoid was used to give the beam an initial deflection. The recorder was started and power to the solenoid cut off to release the beam and record its natural decay curve.

4.2 ROOT EFFECTS

Root effects were studied for the two roots available - fir tree and dovetail. The appropriate disk was rigidly attached to the large steel table. Centrifugal force effects were simulated by loading the blades axially. The electrodynamic shaker was then fixed to the blade near the tip using two rollers in the jig to create a pinned connection. The amount of total damping of the system for various axial loads up to 80 lbs. was determined by the resonance bandwidth method. The system aerodynamic and hysteric damping value was then determined by repeating the above tests with the root rigidly fixed with epoxy resin cement. Root damping was then found by subtraction of the aerodynamic and hysteric damping value from the total damping value at each load. Vibration amplitude was monitored by accelerometer with readout on the vibration meter of the frequency analyzer. Frequency was determined with the digital counter.

5 RESULTS AND DISCUSSION OF THE ANALYSIS

5.1 BLADE EFFECTS

5.1.1 Hysteretic Damping

The curves of tip amplitude against cycles from the start of the test are given in figures 6 to 13. Each curve has results from at least two tests, with good reproducibility of results. The experimental points shown on the graphs represent the maximum tip amplitude of the beam taken from the light-beam recorder output. Thus, the curves as drawn represent the decay curve envelope for each beam.

Values of J and n calculated from the experimental results using equation F may be found in Appendix A. Appendix A, figure 28, shows values of damping capacity for materials tested against stress for a uniformly stressed unit cube calculated from values of J and n found experimentally. Figures 14 and 15 show values of J and n respectively as a function of frequency for 6061-T6 aluminum (beams 1, 2, and 3) in the range of 8 to 200 cps, including results taken from Baker, Woolam and Young (20). Damping capacity for 6061-T6 aluminum is shown to be definitely a function of frequency.

It is obvious that none of the curves, except possibly figure 12, are linear on the semi-log plot which is the situation when $n=2$ representing a special case since equation (D) becomes

$$D = \frac{4Jbh^3E^2}{15l^3} \Delta_{pk}^2 \quad (G)$$

For sinusoidal motion at resonant frequency f_R tip velocity

$$v_{pk} = 2\pi f_R \Delta_{pk}$$

Thus (G) may be written

$$D = \frac{Jbh^3E^2}{15\pi^2l^3f_R^2v_{pk}^2}$$

and damping becomes proportional to velocity squared as in the classical viscous case.

For $n=2$, equation (F) reduces to

$$\frac{1}{\Delta_{pk}} \frac{d\Delta_{pk}}{d(\text{cycle})} = J E f_R$$

which has the solution

$$\ln \Delta_{pk} = J E f_R (\text{cycles}) + \beta$$

where $\beta = \text{constant}$

Since the 'cycle' scale is arbitrary, an initial condition at cycle 1 may be set such that

$$\left[\ln \Delta_{pk} \right]_{\text{cycle}_1} = J E f_R \text{ cycle}_1$$

thus $\beta = 0$ and Δ_{pk} , when plotted to a semi-log scale against cycles, appears linearly dependant on cycles, as is the case with classical viscous damping. This special case occurs in the case of beam no. 7 in figure 12.

It is interesting to note that for $n=2$, the curves are concave up and for $n=2$, the curves are concave down.

The actual energy loss due to hysteretic and aerodynamic damping was calculated from equation E. The results of energy loss against tip amplitude are shown in figures 16 through 23. As expected, the curves indicate that energy dissipation increases exponentially with tip deflection.

Note that in Appendix A figure 28 specific damping capacity for 6061-T6 aluminum at a fixed uniform stress, calculated from experimental values of J and n , exhibits little change from 26 to 216 cps

although material damping constants do depend on frequency in this range. This possibly explains results of some early investigators who found damping to be independent of frequency for certain materials.

5.1.2 Aerodynamic Damping

From the natural decay curves of maximum tip amplitude against cycles from the start of a test taken at atmospheric pressure, figures 6 to 13, total energy loss per cycle as a function of maximum tip deflection was calculated from equation E. From this value the amount of material hysteresis energy loss per cycle at a given maximum tip amplitude was subtracted to yield aerodynamic energy loss per cycle as a function of maximum tip amplitude.

Results of aerodynamic energy loss per cycle as a function of maximum tip amplitude are plotted in figures 16 to 23. Aerodynamic energy loss is not plotted for beam no. 8 since it was negligible. The plots of aerodynamic damping against tip amplitude are collected for all beams tested and plotted to a log-log scale in figure 24. Curves shown are close to linear on the log-log plot verifying the exponential nature of the dependence of aerodynamic damping on tip displacement in the range tested. The exponents relating aerodynamic damping against tip amplitude for beams 1 and 2 show a similar exponent. For the same tip amplitude, the ratio of aerodynamic damping for beams 1 and 2 is the same as the frequency ratio raised to the aerodynamic exponent. However, beam 3 is larger than beam 5 (ie. sweeps a greater volume) and has a higher natural frequency, but at the same tip amplitude, beam no. 3 exhibits less aerodynamic damping than beam no. 5. Hence the relationship between beam width and length and aerodynamic damping is not simply one of swept volume.

The aerodynamic exponents (Appendix A) lie between 2.00 and 3.26. It is of interest to note that none fall below 2.0, which represents the classical viscous case.

Ratios of aerodynamic to material hysteretic energy loss per cycle for the beams tested against tip amplitude are plotted in figure 25. It may be seen that this ratio may increase or decrease with tip amplitude, depending on the ratio of the aerodynamic damping exponent to the material hysteretic damping exponent. For beams 1,3 and 4, the aerodynamic exponent is greater than the hysteretic exponent, hence, aerodynamic damping increases at a greater rate than hysteretic damping as tip amplitude increases. The opposite is true with the other beams. All experimental cases except beam no. 7 exhibited a ratio of aerodynamic to material hysteretic damping in the range of 0 to 200%. The ratio for beam no. 7 was in the range of 700% due to its low hysteretic damping at low stress levels even for large amplitudes as a result of its length and thickness. Beam no. 7 is not shown in figure 25 to maintain a suitable scale.

At higher modes, amplitudes would be decreased significantly. The exponential nature of aerodynamic energy loss indicates that at modes higher than the first flexural, aerodynamic energy loss should be insignificant.

5.2 ROOT EFFECTS

Logarithmic decrements, as obtained from equation (B), against load are plotted in figure 26 for the dovetail root. The axial load has been converted to the angular speed required to create an equivalent centrifugal load. Results for the fir tree root tested are not shown since significant axial loads could not be applied using the apparatus.

Figure 26 also shows results for several types of roots as found by Hanson, Meyer and Manson (22). The results found agree in order of magnitude with these values. As shown, damping decreases significantly with rpm, due to the second order root tightening effect of centrifugal forces, except for the pin root which dissipates energy by rolling as well as by sliding. The curves of figure 26 do not approach zero damping asymptotically as speed increases indicating that linear or coulombic damping does not exist. This figure also indicates the relatively small amounts of energy which may be dissipated in the root at high rpm. The blades used in these tests normally operate at a design speed of 35,000 rpm, hence little or no damping results due to root geometry. It is interesting to note the suggested results for pin connected blades are an order of magnitude greater than for sliding friction type roots.

At low equivalent rotational speed, root damping log decrements were found as high as 6%. Due to aerodynamic or hysteretic damping, maximum log decrements found in the range tested were in the range of 8%, with most values in the range of 0.3 to 1.0%.

5.3 ESTIMATE OF EXPERIMENTAL ERRORS

Errors are considered in two parts

- i) Assumptions
- ii) Transducer and readout equipment

Assumption Errors

Minimum jig to specimen weight ratio was 90, with a maximum value of 1,120. Reference 29 suggests this ratio should be greater than 100, but no induced experimental error is estimated from these tests.

For most tests, the log decrement value is less than 1% and maximum values were 8% in the ranges used. Thus, damping was small, that is, the ratio of energy loss per cycle was always less than 16% and usually less than 2%. Hence, maximum strain energy could be calculated either before or after the cycle in question, although the mean value was used in this case.

The continuity of damping is shown by the smooth continuous curves of both aerodynamic and material hysteretic damping as functions of tip amplitude.

Figure 27 shows a typical plot of a beam (no.4) deflection profile. The amplitudes were measured by accelerometers and non-dimensionalized with the tip displacement. This figure also shows the static non-dimensional displacement curve under a uniform load as calculated from elementary beam theory. Agreement between the static and dynamic case was found within 2%, which is within the readout accuracy of the accelerometers. This agreement indicates that the effects of shear deflection and rotary inertia in the dynamic case were negligible.

Beams vibrated in a pure first flexural mode at all times during tests. This was illustrated by observation of strain gage or accelerometer output signals on an oscilloscope. Traces at all times showed little or no distortion on the signal due to noise or complex vibrations, except for the first few cycles after release of the load in the natural decay tests. These first few cycles were disregarded in data analysis.

No attempt was made to monitor dynamic modulus of elasticity.

254464

This would essentially require determination of material hysteresis loops. Since energy dissipations are small, this measurement requires highly precise equipment. Lazan (14) (15) has suggested that at room temperature, the dynamic modulus is essentially the same as the static modulus. There is no reason to doubt that this is not the case in present work.

No differences could be observed in decay curves taken at one and four psia, thus it is believed that aerodynamic damping is negligible at pressures less than one psia.

Energy dissipation in the strain gage is difficult to estimate. Although the gages were placed in high stress areas, they did not cover large areas of the beams and their effect is believed to be small.

Beams were initially cycled several million cycles to remove any virgin material effects. This was done in the forced vibration apparatus. Beams were run at constant input energy until tip deflection was stable.

During a series of decay tests on a given beam, no variation in material hysteretic damping constants J and n was noticeable. Thus it is believed that no error is introduced by the assumption that material hysteretic damping constants remained constant for a given beam over the duration of the tests.

The maximum tip deflection of each beam was monitored at all times by either an accelerometer or a strain gage. On no occasion was the tip deflection allowed to exceed a value which would cause the maximum stress in a beam to exceed the cyclic stress sensitivity limit. Thus no error was introduced at any time due to stresses

exceeding the cyclic stress sensitivity limit.

27

The small amount of energy dissipated in a blade was easily dissipated to the surroundings, resulting in no significant blade temperature rise. Errors in strain gage output due to thermal effects are thus judged as negligible.

Transducer and Readout Errors

Accelerometers, including supplied cables, are individually calibrated by the manufacturer to a suggested accuracy of $\pm 2\%$ with flat frequency response within 2% from 2cps to 25 kcs with stability better than 2% per year. Miniature accelerometers, as used on test specimens weigh 0.07 oz. This represents 6% of the weight of beam no.2 but is less than 1.4% in all other cases. Elementary beam natural frequency theory suggests that the effective mass of the accelerometer is 24% of its true mass. Thus, the error in neglecting the effect of accelerometers in both frequency and displacement is considered very small.

The digital counter is accurate to ± 1 cps in the range used, based on an internal calibration test.

For the light beam recorder output, Appendix C figure 30, frequency could be determined to $\pm 1\%$. Frequency response of the combined carrier amplifier - recorder system as used is flat within 3% from 10 to 400 cps., based on both manufacturer's specifications and actual tests. Strain amplitude could be read to within $\pm 1\frac{1}{2}\%$ of full scale deflection. At least two tests were run on each natural decay tests. Repeatability was within limits of experimental accuracy.

Since slopes were required for the separation of material damping constants, J and n, larger errors were introduced. To minimize

probable errors, J and n were calculated for at least ten positions along the curve in question and then averaged, but the maximum possible error for an individual calculation is $\pm 10.9\%$ for n and $\pm 33.4\%$ for J .

The aerodynamic exponent could be determined within $\pm 5\%$.

Maximum strain energy could be determined within $\pm 9.7\%$. Energy loss per cycle could be determined within $\pm 9.9\%$ and logarithmic decrements, from equation (B), to within $\pm 7\%$. The error involved in the assumption that equation (B), developed for a classical viscous case, is valid for the experimental case is not evaluated.

Using forced vibration tests to determine aerodynamic and hysteretic damping log decrements, hence energy loss and ultimately material damping constants, introduced unacceptable errors and this approach was abandoned.

Forced vibration tests were also found to be unsatisfactory for determination of energy dissipation in cantilever beams since attempts to measure energy input to the beams, which is equal to energy dissipation, proved unsatisfactory due to the extremely small values involved.

6 RECOMMENDATIONS

6.1 SUGGESTIONS FOR EXPERIMENTAL IMPROVEMENT

The use of a much larger shaker table and the associated larger power amplifier with an extremely sensitive and accurate input energy monitoring system would allow forced vibration tests to be used to determine damping properties. This would also allow steady-state forced vibration analysis at high stress levels as well as analysis of the effect of large numbers of cycles on damping constants.

The use of constant-stress beams would simplify the analysis theoretically for the determination of material damping constants.

A non-contacting, full-field method of determining blade deflections would allow simple verification of theoretical deflection analysis of complex shaped blades. A possible method is that of holographic interferometry.

The use of a pressure chamber as well as a vacuum chamber would allow determination of aerodynamic effects at pressures higher than atmospheric.

A displacement transducer which is more sensitive than the accelerometers used would allow analysis of off-resonance vibration where displacements are much smaller than at resonance.

6.2 SUGGESTIONS FOR FURTHER WORK

The determination of damping constants for other materials of the type used in turbine blading in the frequency range of 100 cps to approximately 20 kcs. would be valuable. The effects of prestress and high damping capacity coatings on blading is also of interest.

An aerodynamic study could determine the relative magnitudes of sources of aerodynamic damping.

In terms of root damping, further work might include the effects of sub-platform dampers as well as the use of pin connected roots. A visco-elastic shear damper may be found which could increase root damping by several orders of magnitude if the material would survive in the actual engine environment.

7. CONCLUSIONS

1) Experimentally, values of material hysteretic damping constants have been found for the materials tested in the frequency ranges used.

2) Material hysteretic damping constants have been shown to be a function of frequency in the range tested.

3) Material hysteretic damping for a blade has been shown to be a function of material, frequency and stress distribution (ie. geometry and deflection profile) and to increase exponentially with stress.

4) Natural decay tests conducted in a vacuum chamber and in air allow separation of material hysteretic damping from aerodynamic damping in still air. For the beams tested, negligible aerodynamic damping was found at pressures less than one psia at room temperature.

5) In still air, as found under stall conditions when vibratory exciting forces generally are large, aerodynamic damping has been shown to be of the same order of magnitude as material hysteretic damping in the first flexural mode.

6) Aerodynamic damping in still air has been shown to be a function of blade geometry, vibratory amplitude (or velocity) and increases exponentially with blade vibratory amplitude (or velocity) at a given frequency.

7) While root damping may be significant at low rotational speed, it decreases rapidly as rotational speed increases and may be negligible at full operating speed. Root damping will, however, be very effective in suppressing vibrations during engine start-up.

BIBLIOGRAPHY

1. Smith, J. E., "The Vibration of Blades in Axial Turbomachinery",
A. S. M. E. paper 66-WA/GT-12
2. Carta, F. O., "Coupled Disk - Blade - Shroud Flutter Instabilities
in Turbojet Engine Rotors", A. S. M. E. paper 66-WA/GT-6
3. Bury, K. V., "A Method of Calculating and Designing for a Minimum
Vibration of Turbomachinery Blades", A. S. M. E. paper
67-VIBR-49
4. Armstrong, E. K., and Stevenson, R. E., "Some Practical Aspects of
Compressor Blade Vibration", Journal of the Royal Aeronautical
Society, Vol. 64, March, 1960, p. 117-130
5. Chubb, S. B., "Evaluation of Wire Lacing for the Control of Gas
Turbine Blade Vibration", A. S. M. E. paper 67-VIBR-47
6. Kimball, A., "Internal Friction in Solids", A. S. M. E. Transactions,
Vol. 48, 1926, p. 479
7. Kimball, A. and Lovell, D., "Internal Friction in Solids", Physical
Review, Vol. 30, 1927, p. 948-959
8. Cranfield, R., "Internal Friction in Metals", Physical Review, Vol.
32, 1928, p. 520-530
9. Kimball, A., "Vibration Damping Including the Case of Solid
Friction", A. S. M. E. Transactions, Vol. 51, 1929, p. APM-
51-21-227
10. Dorey, S. F., "Elastic Hysteresis in Crank Shaft Steels", Institution
of Mechanical Engineers - Proceedings, Vol. 123, 1932, p. 479-510

11. Robertson, J., and Yorgiadis, A. J., "Internal Friction in Engineering Materials", A. S. M. E. Journal of Applied Mechanics, Vol. 68, 1946, p. A137-A182
12. Marin, J., and Stulen, F. B., "A New Fatigue Strength - Damping Criterion for the Design of Resonant Members", A. S. M. E. Journal of Applied Mechanics, 1947, p. A209-A212
13. Lazan, B. J., "Damping Capacity of Mild Steel", Proc. A. S. M., Vol. 42, 1950, p 499-558
14. Lazan, B. J., and Demer, L. J., "Damping, Elasticity and Fatigue Properties of Temperature Resistant Metals", Proc. A. S. T. M., Vol. 51, 1951, p. 611-648
15. Lazan, B. J., et al, "Dynamic Testing of Materials and Structures with a New Resonance Vibration Exciter and Control", Proc. A. S. T. M., Vol. 52, 1952 p.858-875
16. Lazan, B. J., "Effect of Damping Constants and Stress Distribution on the Resonance Responce of Members", A. S. M. E. Journal of Applied Mechanics, Vol. 75, 1953, p. 201-209
17. Marin, J., Mechanical Properties of Engineering Materials, Prentice-Hall Inc., 1962, p. 272-293
18. Soroka, W., "Hysteretically Damped Vibration Absorber and Equivalent Electrical Circuit", Experimental Mechanics, Vol. 5 #2, 1965, p. 53
19. Kavanagh, P., and Serovy, G., "Through Flow Solution for Axial-Flow Turbomachine Blade Rows", N. A. S. A. CR-363, 1966
20. Baker, W. E., Woolam, W. E. and Young, D., "Air and Internal Damping of Thin Cantilever Beams", International Journal of Mechanical Sciences, Vol. 743, 1967, p. 743-766

21. McWithey, R., "Damping Characteristics of Built-Up Cantilever Beams in a Vacuum Environment," N.A.S.A. TN-D 3065
22. Hanson, M.P., Meyer, A.J. and Manson, S.S., "A Method of Evaluating Loose-Blade Mounting as a Means of Suppressing Turbine and Compressor Blade Vibration", Experimental Stress Analysis, Vol.X, no. 2, 1952, p.103-116.
23. Durelli, A.J., Dally, J.W. and Riley, W.F., "Stress and Strength Studies on Turbine Blade Attachment " , Experimental Stress Analysis, Vol. 16 no.1, 1958, p 171.
24. Goodman, L.E. and Klumpp, "Analysis of Slip Damping with Reference to Turbine Blade Vibration", A.S.M.E. Journal of Applied Mechanics, Vol. 78, 1956 p. 421-429.
25. Goatham, J.I. and Smailes, G.T., "Some Vibration Characteristics of Pin-Fixed Compressor Blades", A.S.M.E. paper 66-WA/GT-4.
26. Manson, S.S. et al, Factors Affecting Vibration of Axial Flow Compressor Blades, Experimental Stress Analysis, Vol. 7, no.2, 1949, p.1-15.
27. Drew, D.A., "Measurement of Turbine Stresses in Aircraft Engines in the Laboratory, on the Test Bed, and in Flight", Experimental Stress Analysis, Vol. 10 no.1 p. 187.
28. Timoshenko, S., Vibration Problems in Engineering, 3rd. Edn., Van Nostrand, New York, 1955.
29. Vuksta, T., "Experimental Techniques and Fixture Design Related to Steam Turbine Blade Frequency Measurements", Experimental Stress Analysis, Vol 20 no. 2, 1963, p.161.
30. Lord Rayleigh, Theory of Sound, 2nd edition, MacMillan, New York, p.293-294.

31. Carnegie, W. and Thomas, J., "Natural Frequencies of Long 34
Tapered Cantilevers", Aeronautical Quarterly, November 1967,
p.309- 320.
32. Carnegie, W., "Vibration Characteristics of Turbine Blading",
The Engineer, Vol. 224, n5831, Oct. 27, 1967, p. 545-547.

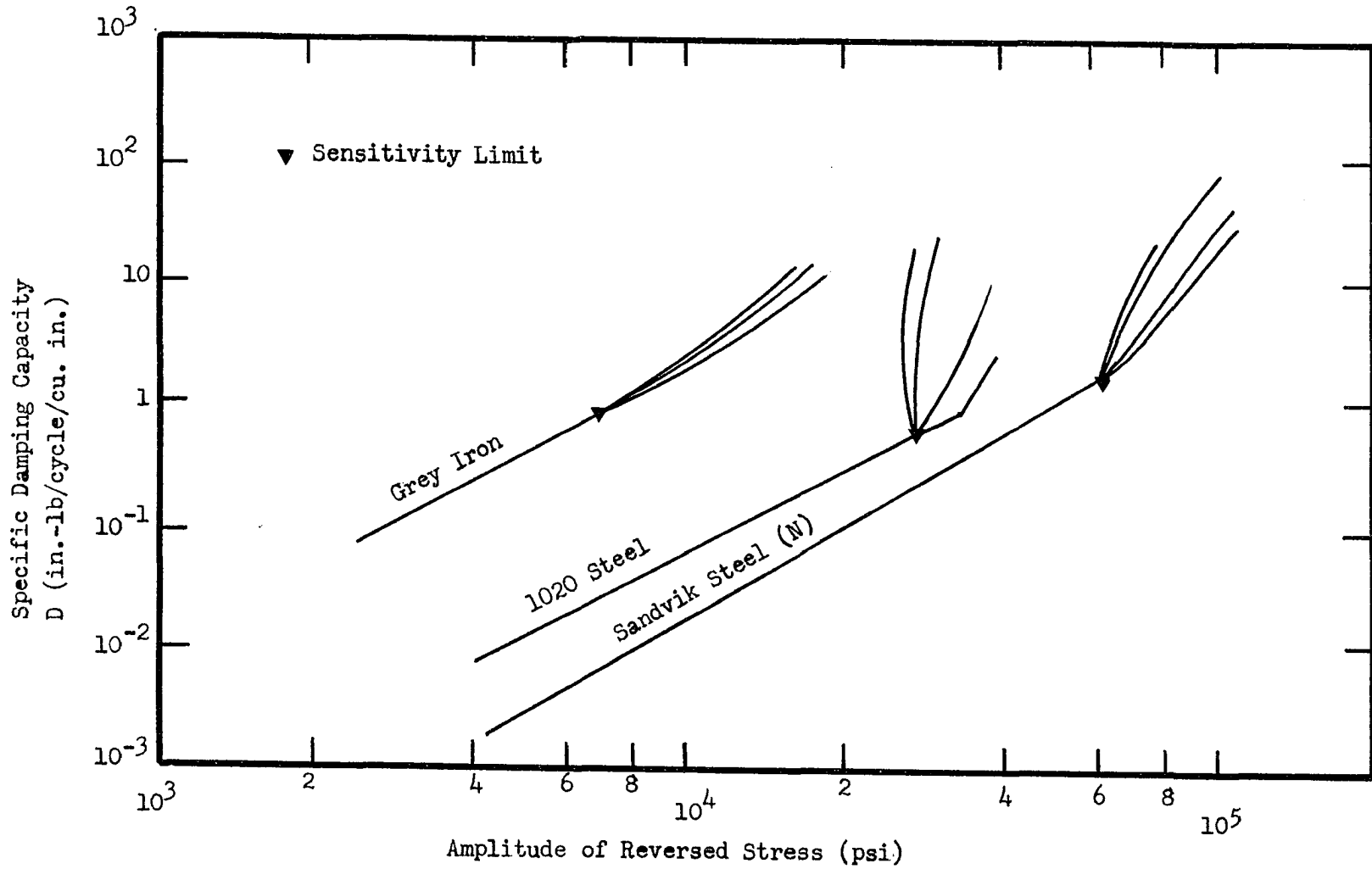


Fig. 1. Specific Damping Capacity against Amplitude of Reversed Stress (20 cpm.)
(From ref.17)

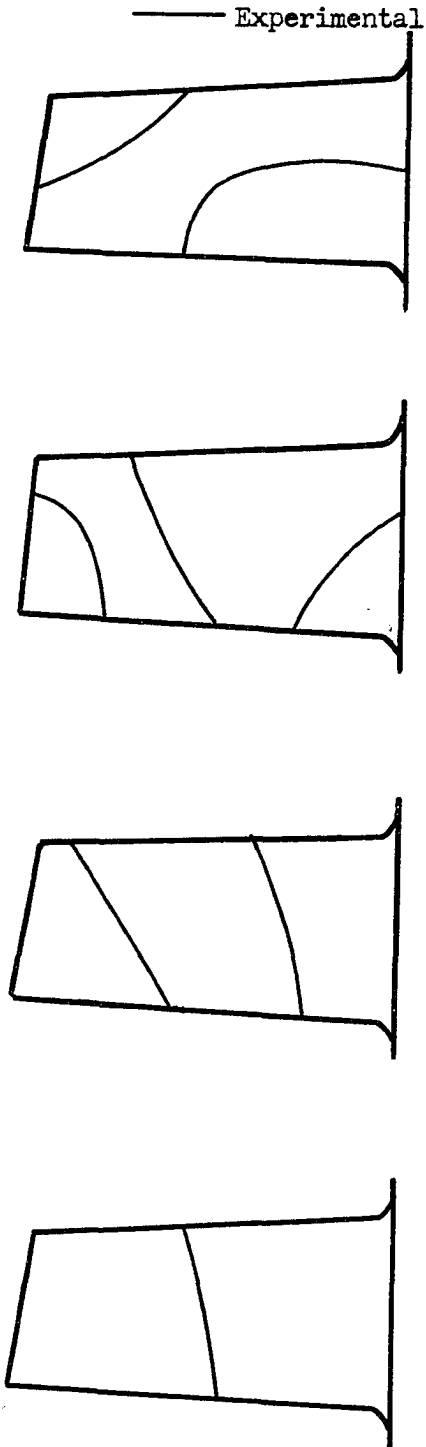


Fig. 2. Typical Nodal Patterns for a Compressor Blade

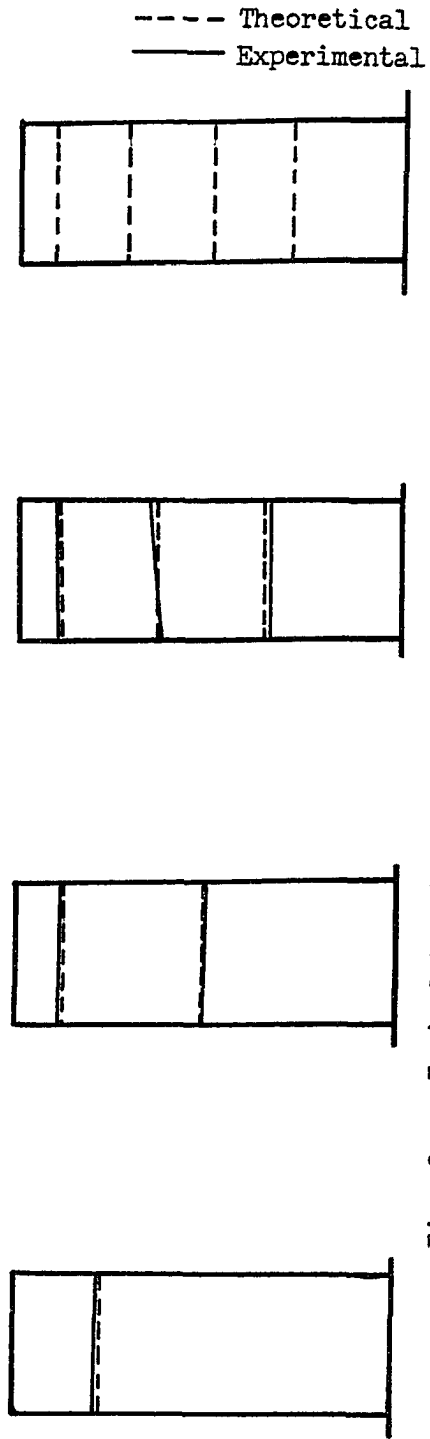
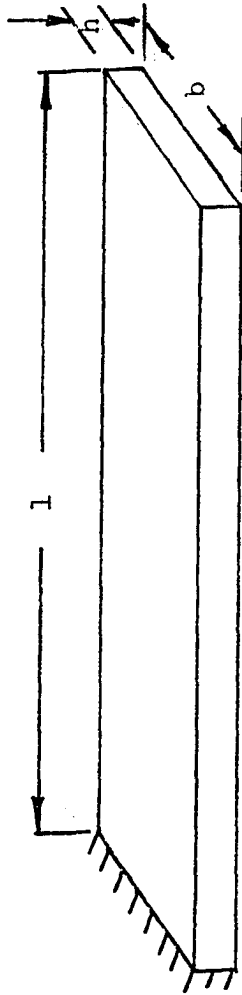


Fig. 3. Typical Nodal Patterns for a Uniform Cantilever



BEAM NO.	1	2	3	4	5	6	7	8
MATERIAL	6061-T6	6061-T6	6061-T6	BRASS	BRASS	304 SS	304 SS	STEEL
h	0.25	0.10	0.10	0.25	0.25	0.25	0.25	0.25
b	1.50	1.50	1.88	1.00	1.00	1.50	1.50	1.50
l	6.00	6.00	11.0	6.00	11.0	6.00	11.0	6.00

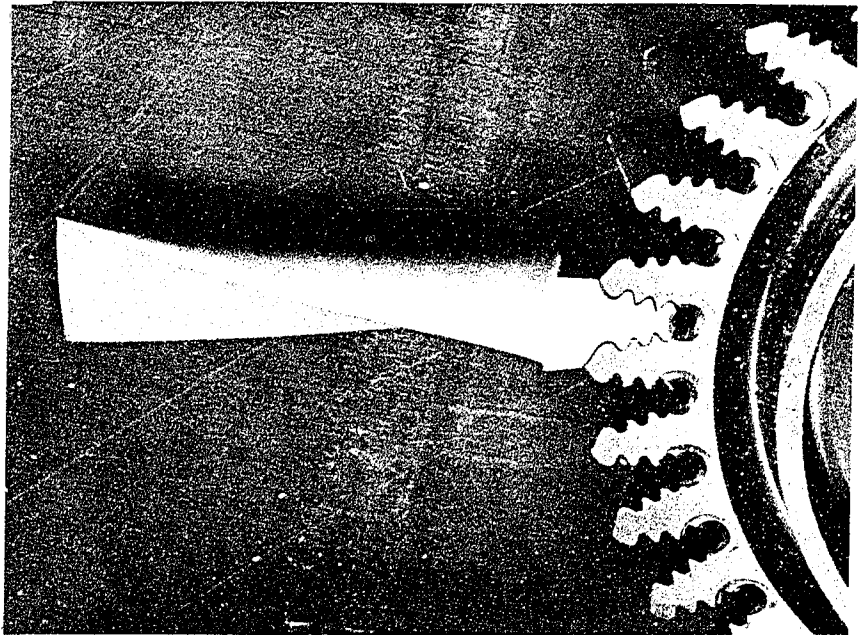
NOTES: 1) All dimensions in inches

2) Tolerances h 0.001"

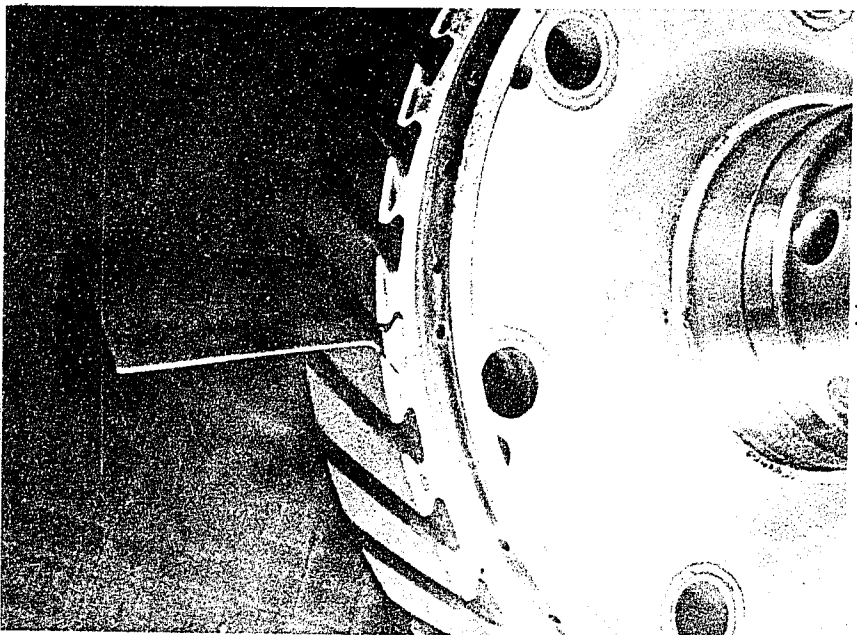
b 0.001"

l 0.003"

Fig. 4. Beam Geometries Studied



FIR TREE



DOVETAIL

Fig. 5. Root Sections Studied

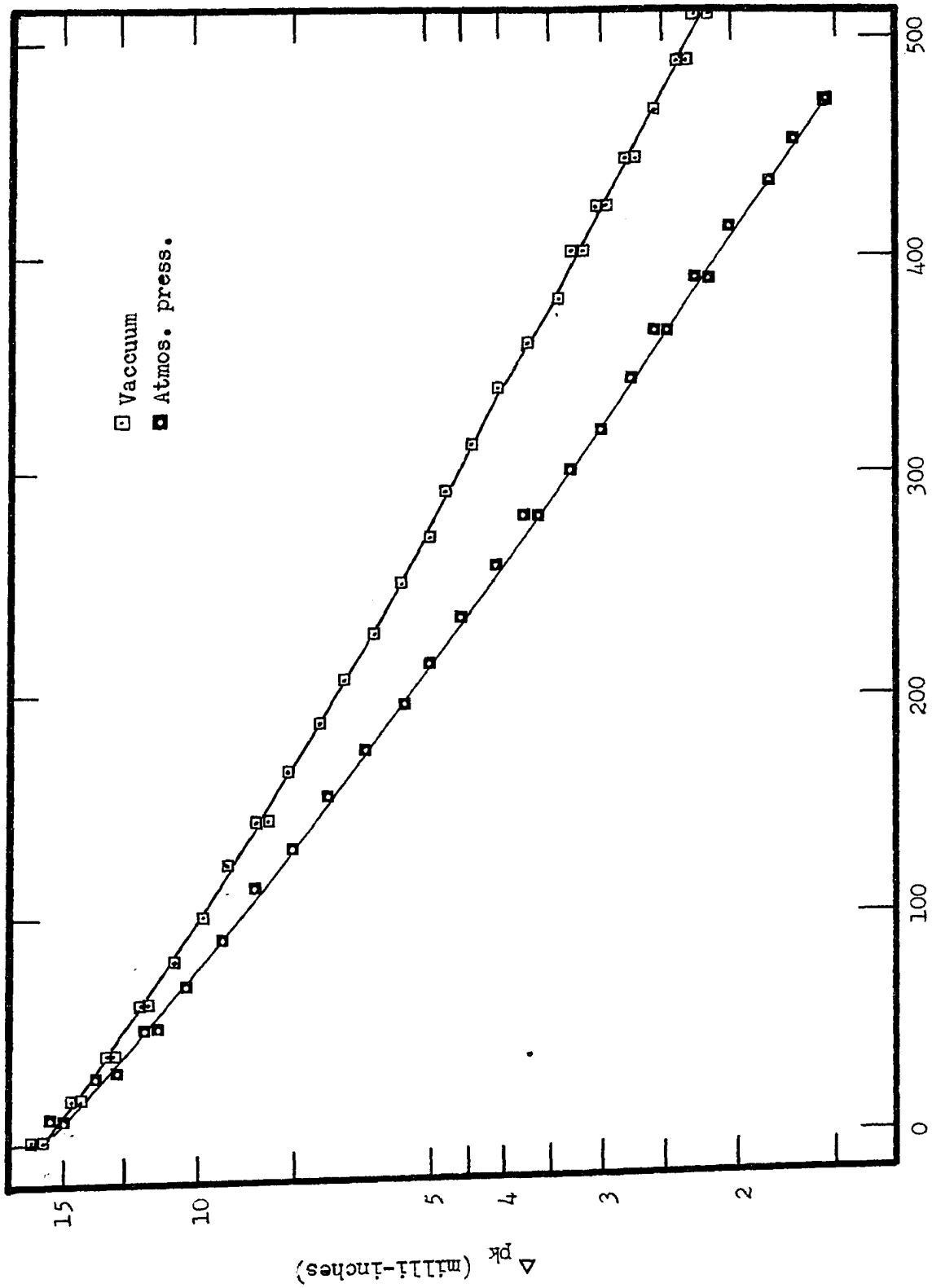


Fig. 6. Beam no. 1. Natural Decay Test-- Tip Deflection against Cycles

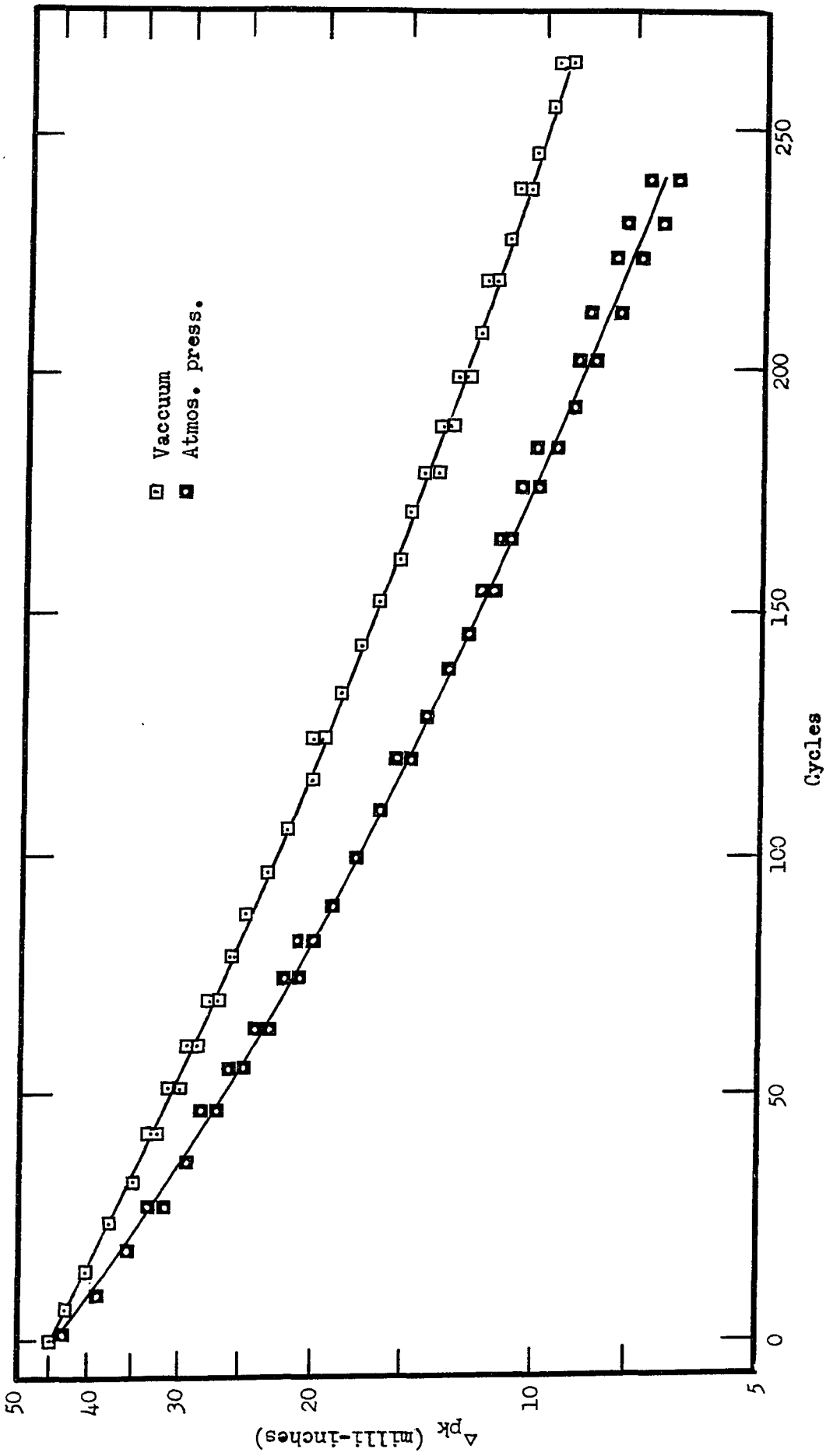


Fig. 7. Beam no. 2. Natural Decay Test - Tip Deflection against Cycles

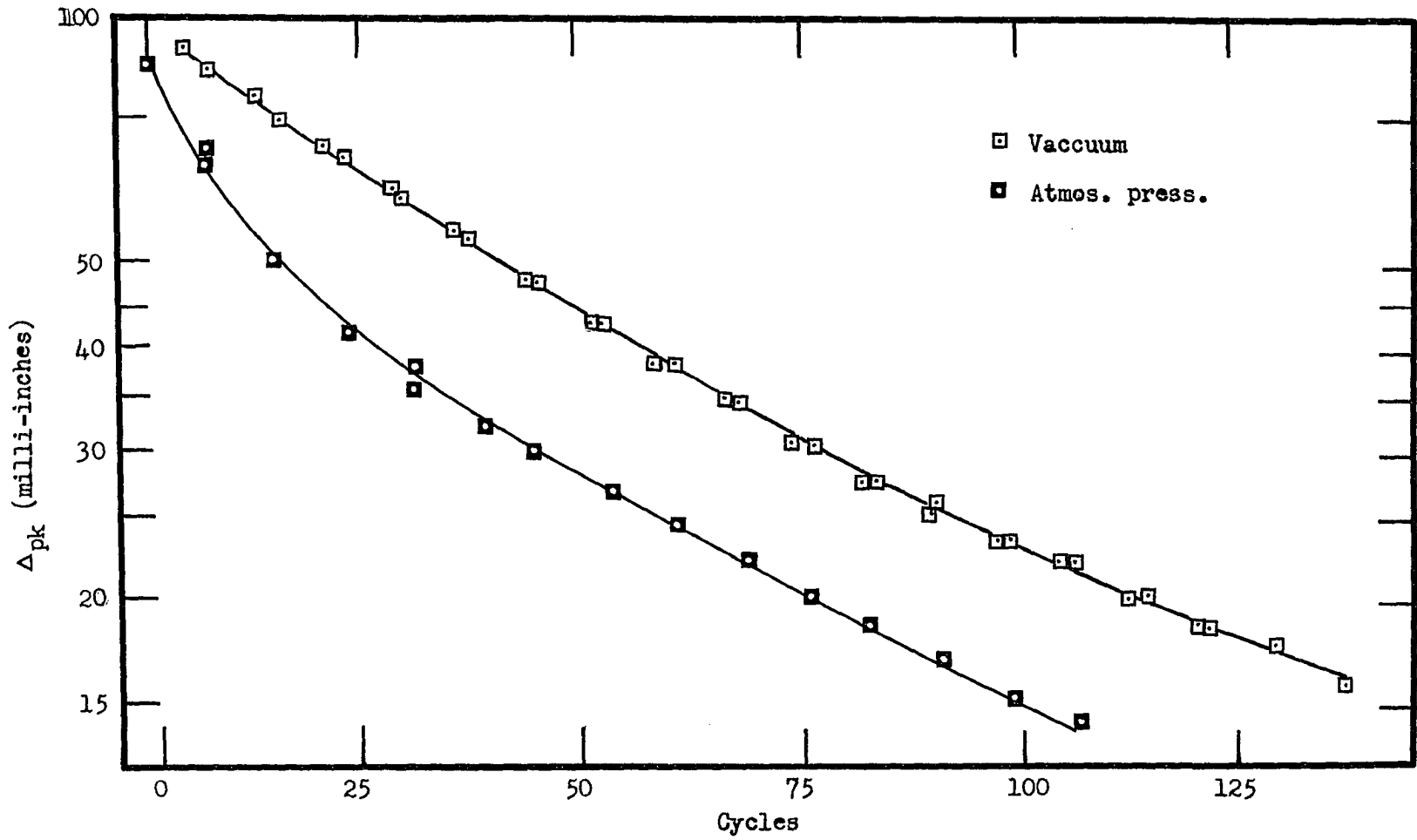


Fig. 8. Beam no. 3. Natural Decay Test - Tip Deflection against Cycles

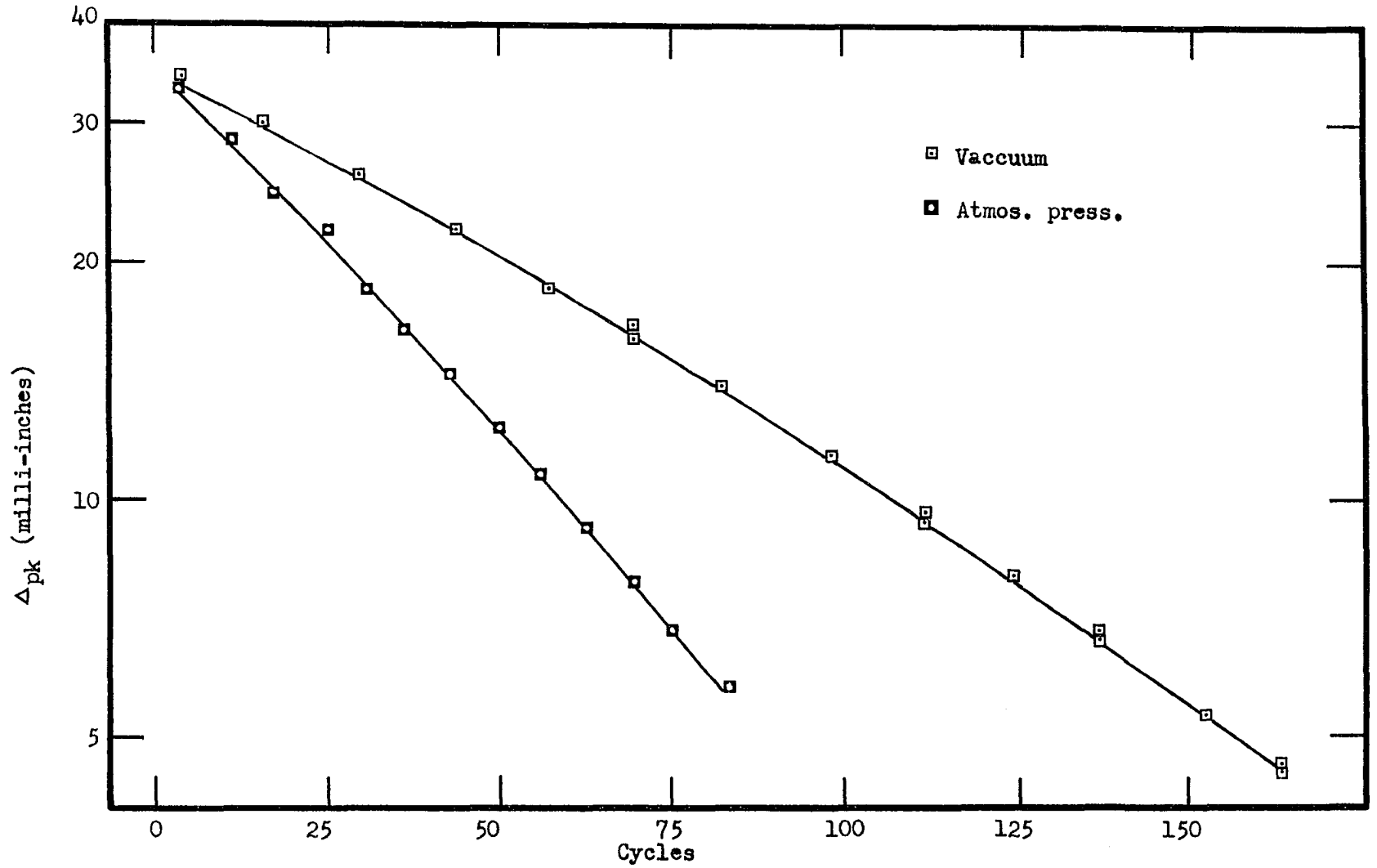


Fig. 9. Beam no. 4. Natural Decay Test - Tip Deflection against Cycles

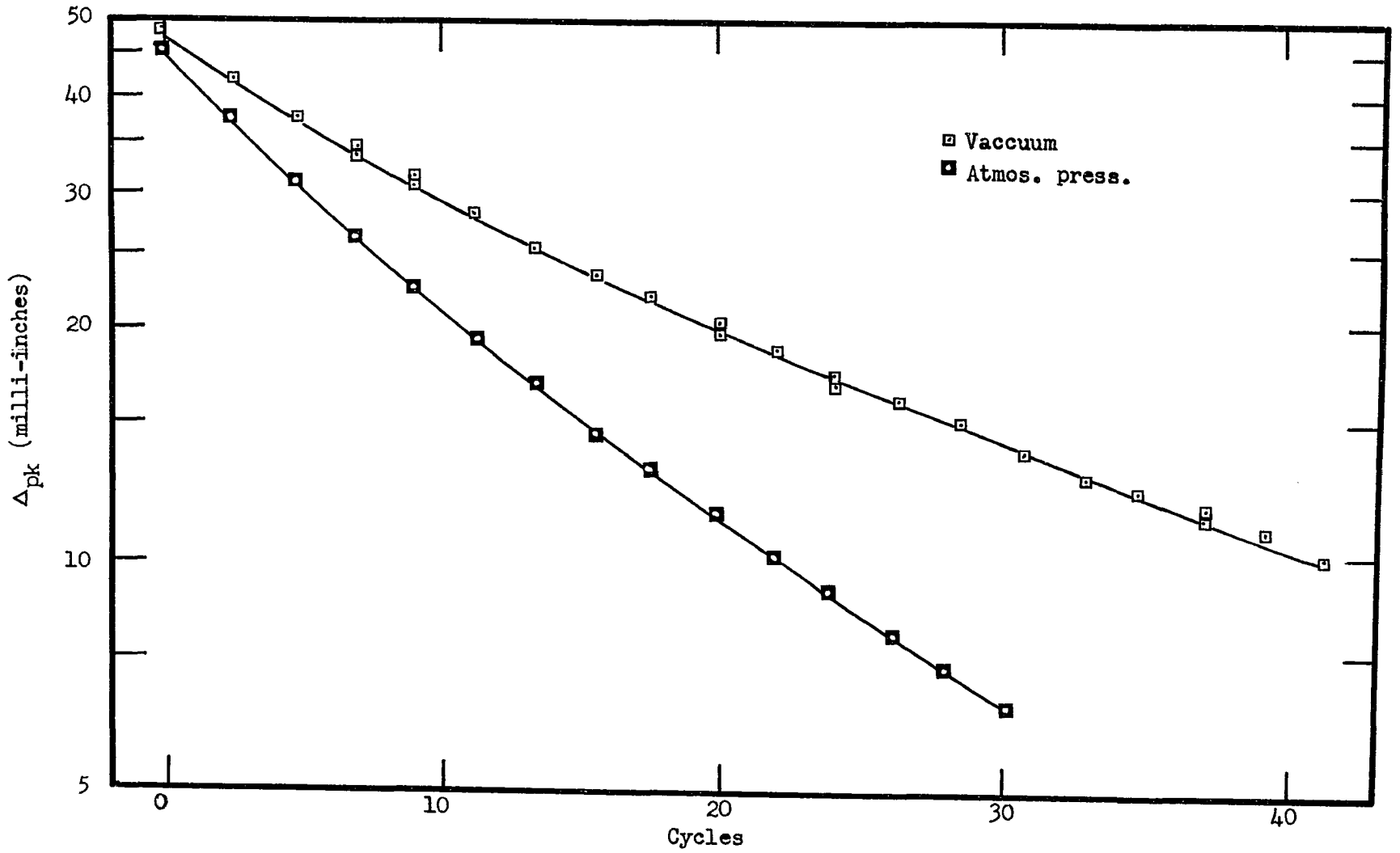


Fig. 10. Beam no. 5. Natural Decay Test - Tip Deflection against Cycles

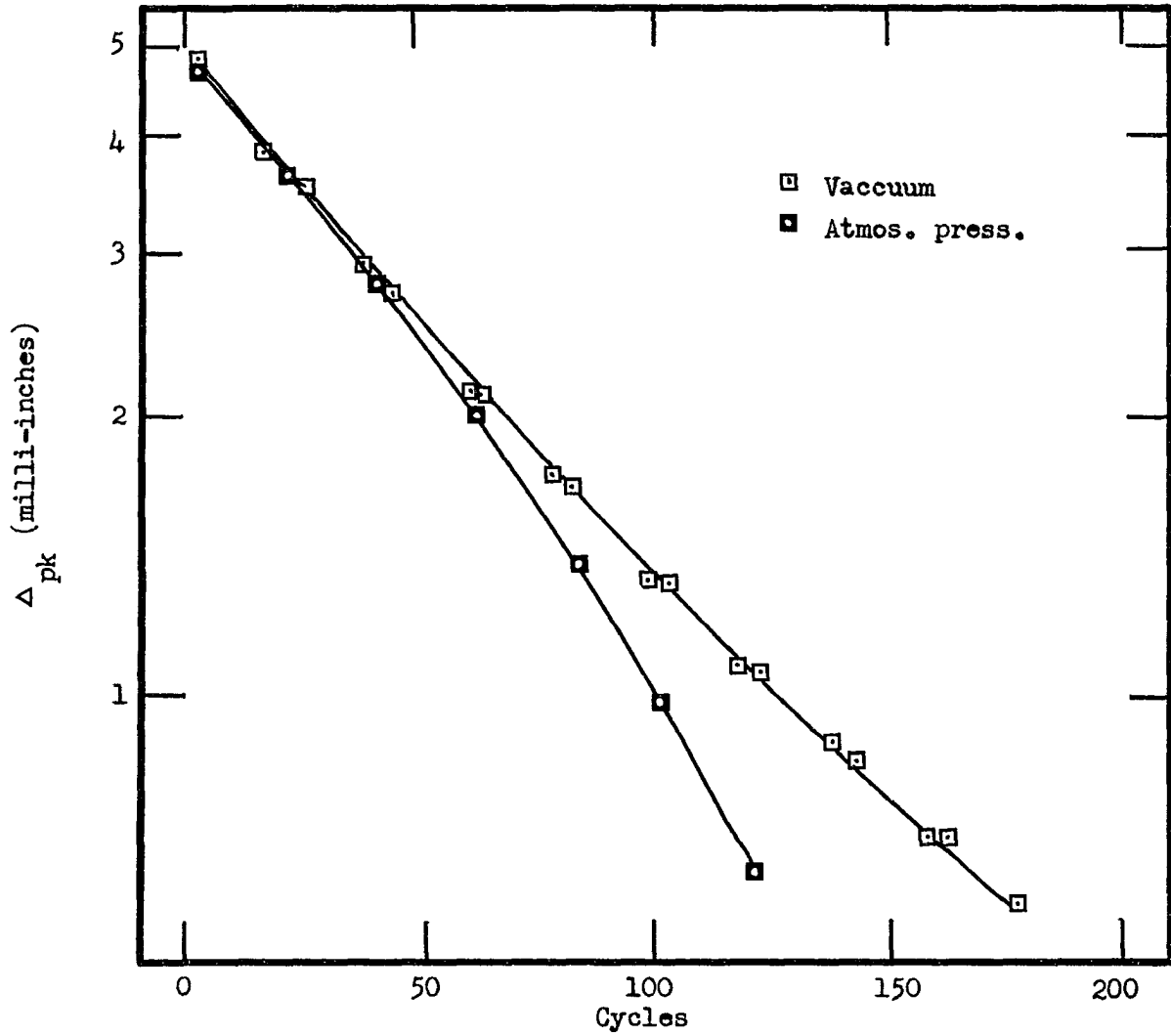


Fig. 11. Beam no. 6. Natural Decay Test - Tip Deflection against Cycles

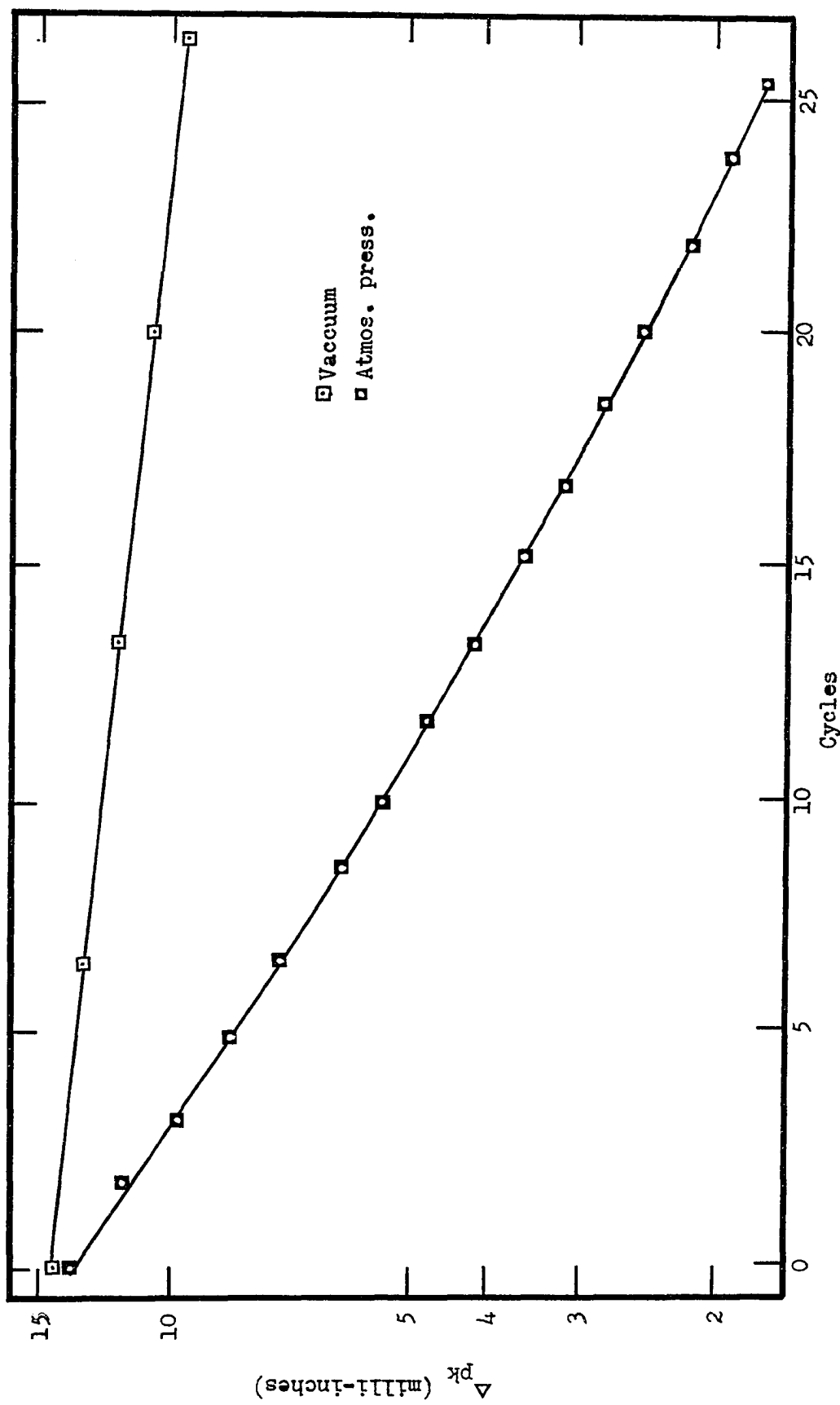


Fig. 1.2. Beam no. 7. Natural Decay Test -- Tip Deflection against Cycles

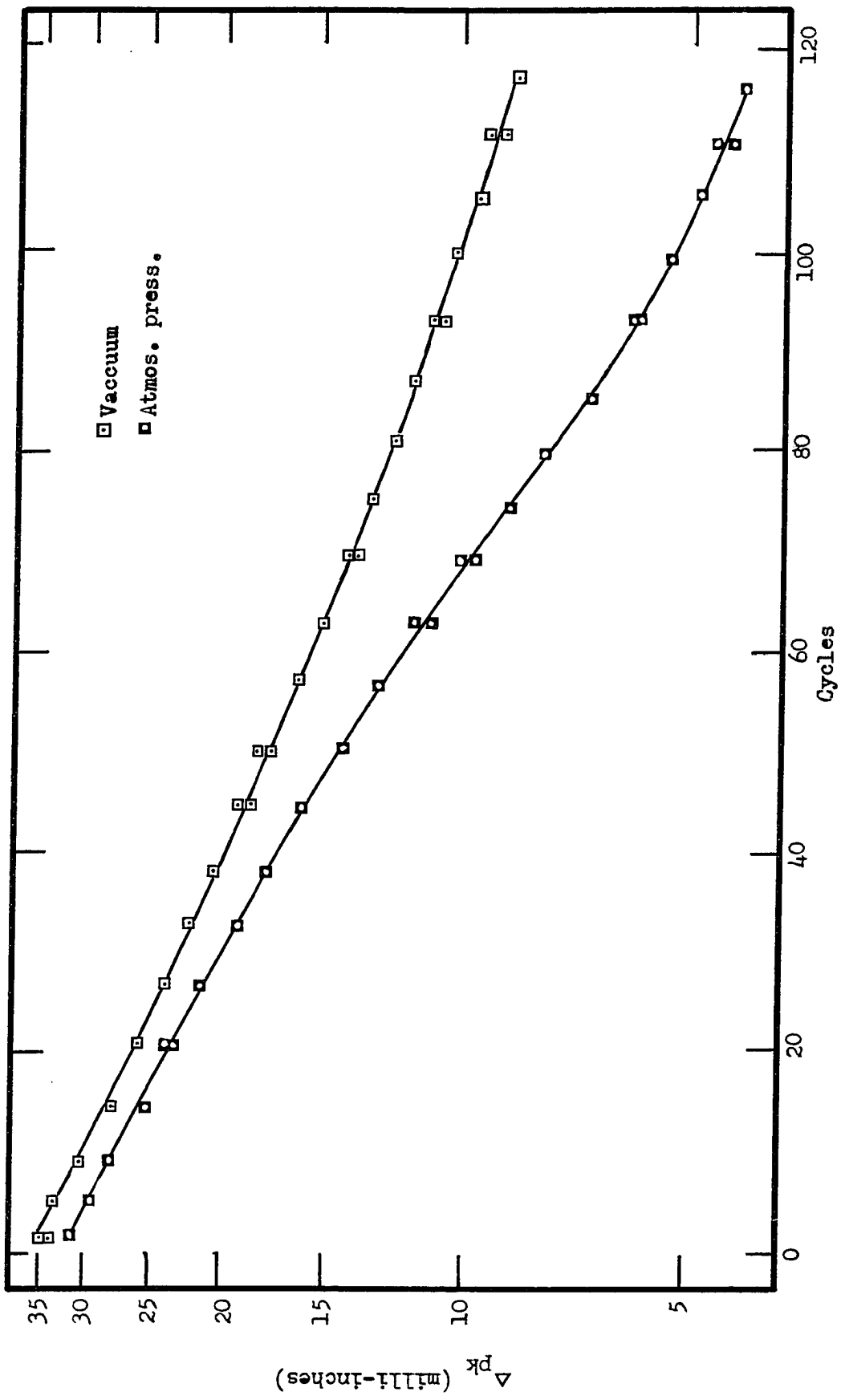


Fig. 13. Beam no. 8. Natural Decay Test - Tip Deflection against Cycles

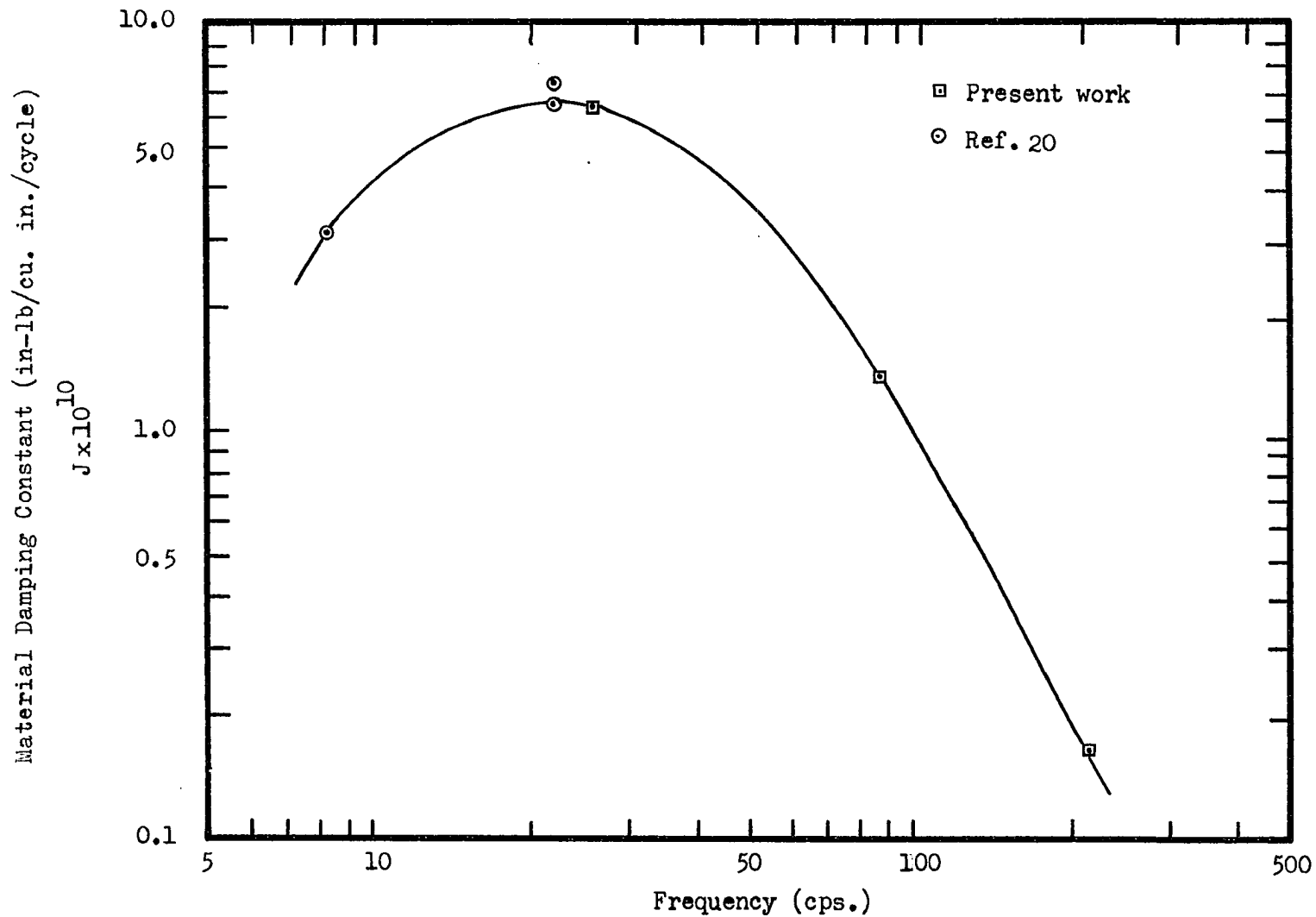


Fig. 14 Frequency Dependence of Material Damping Constant J for 6061-T6 Aluminum

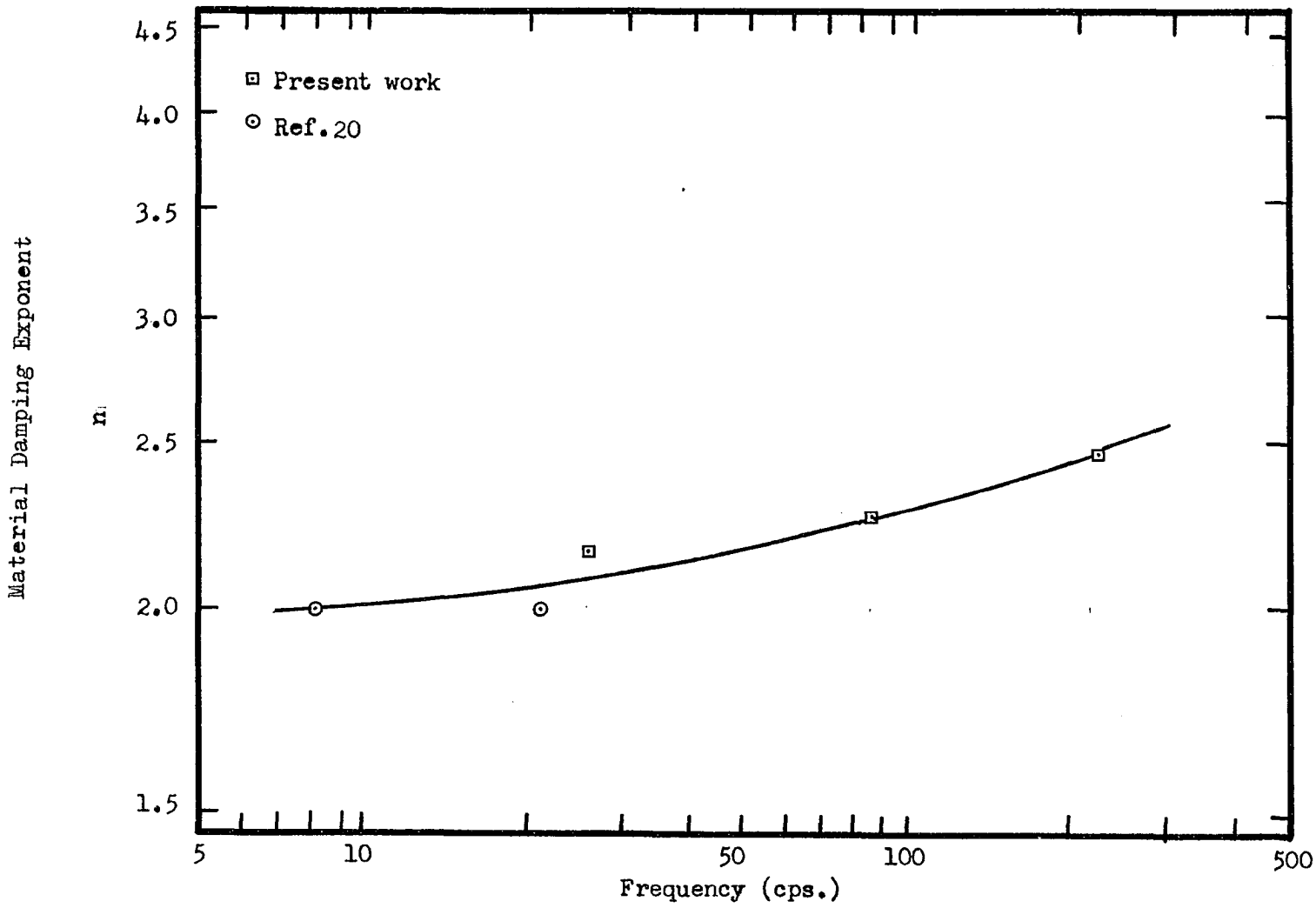


Fig. 15 Frequency Dependence of Material Damping Exponent n for 6061-T6 Aluminum

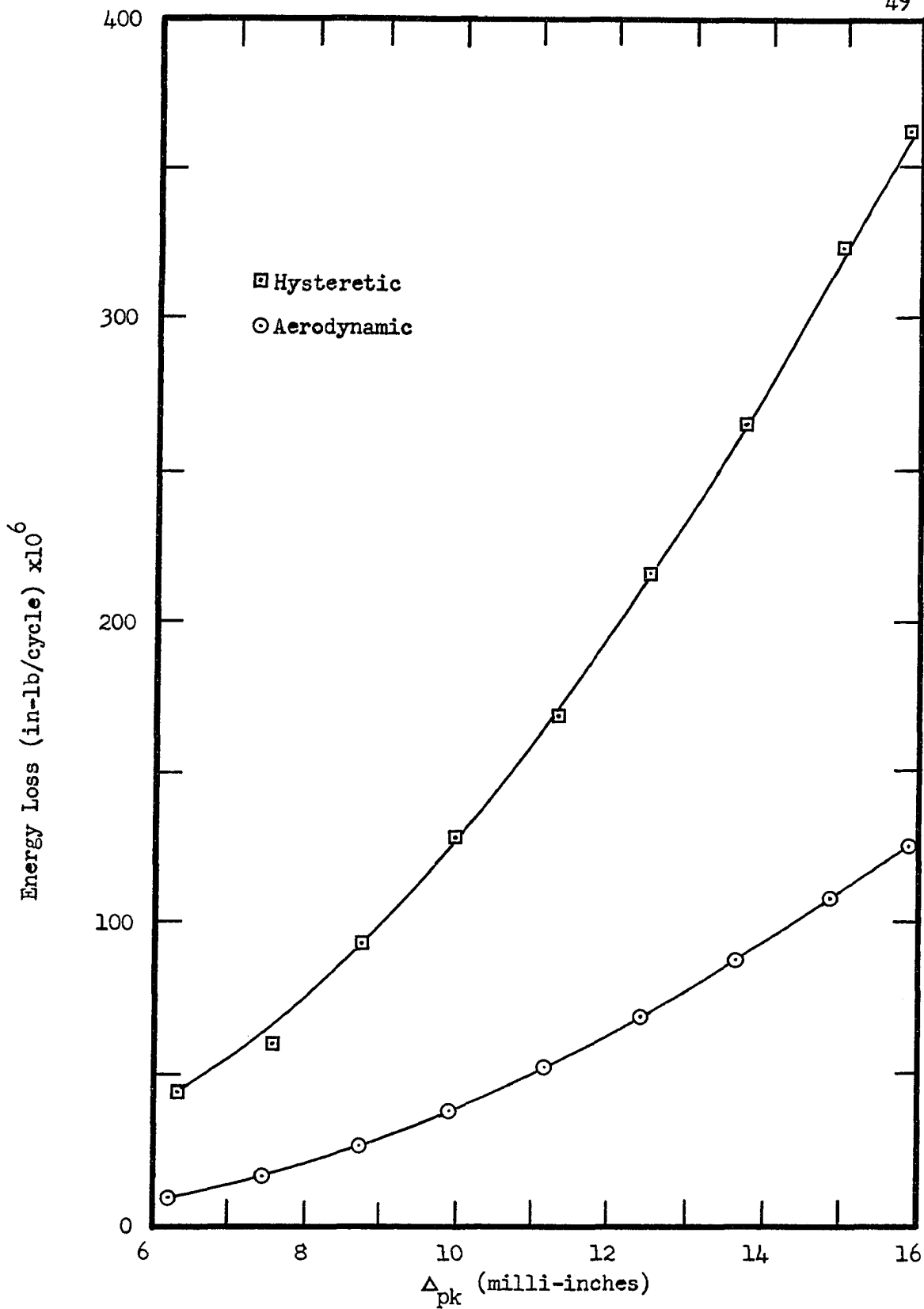


Fig. 16 Beam no. 1. Energy Loss against Tip Deflection

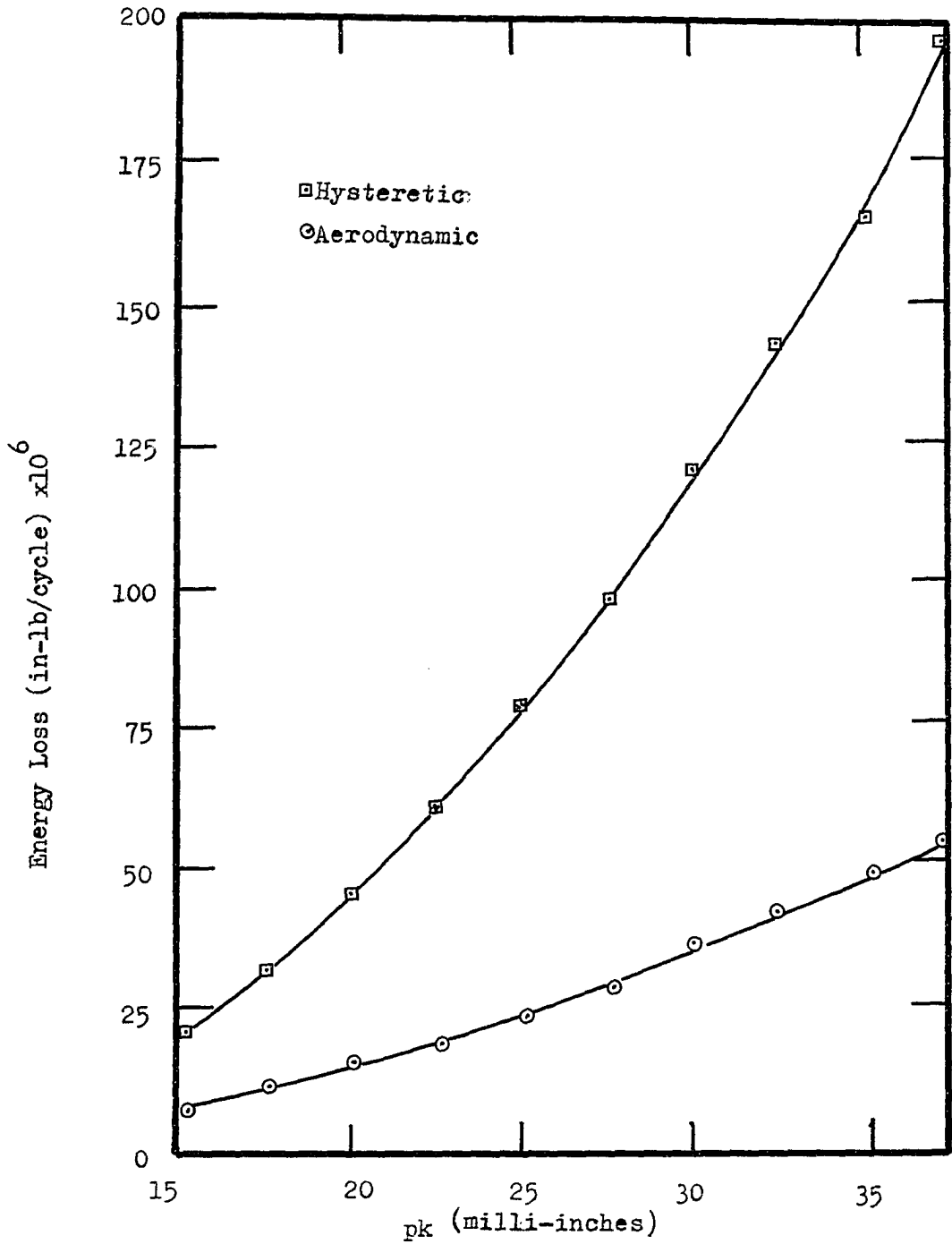


Fig. 17 Beam no. 2. Energy Loss against Tip Deflection.

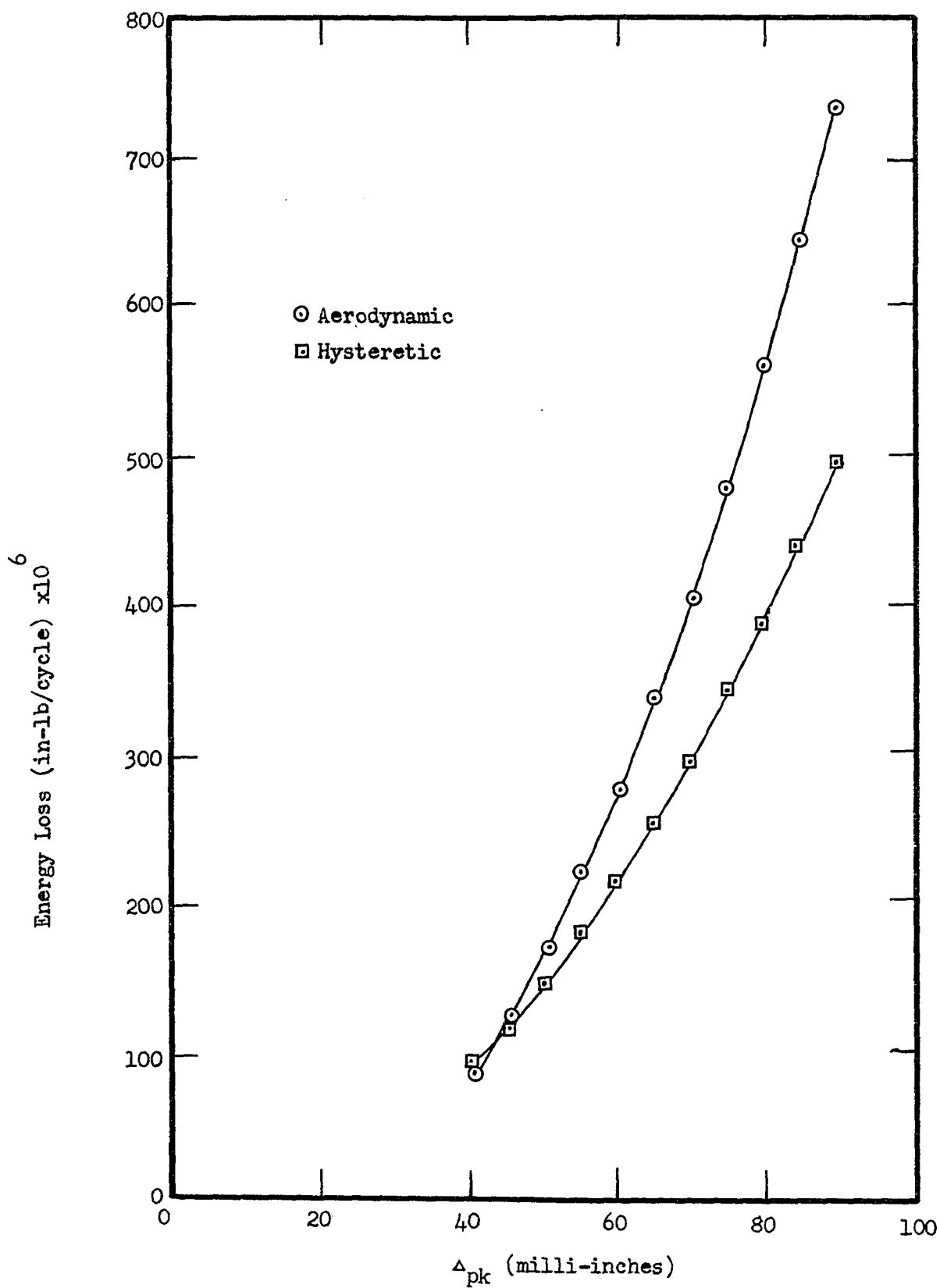


Fig. 18 Beam no. 3. Energy Loss against Tip Deflection

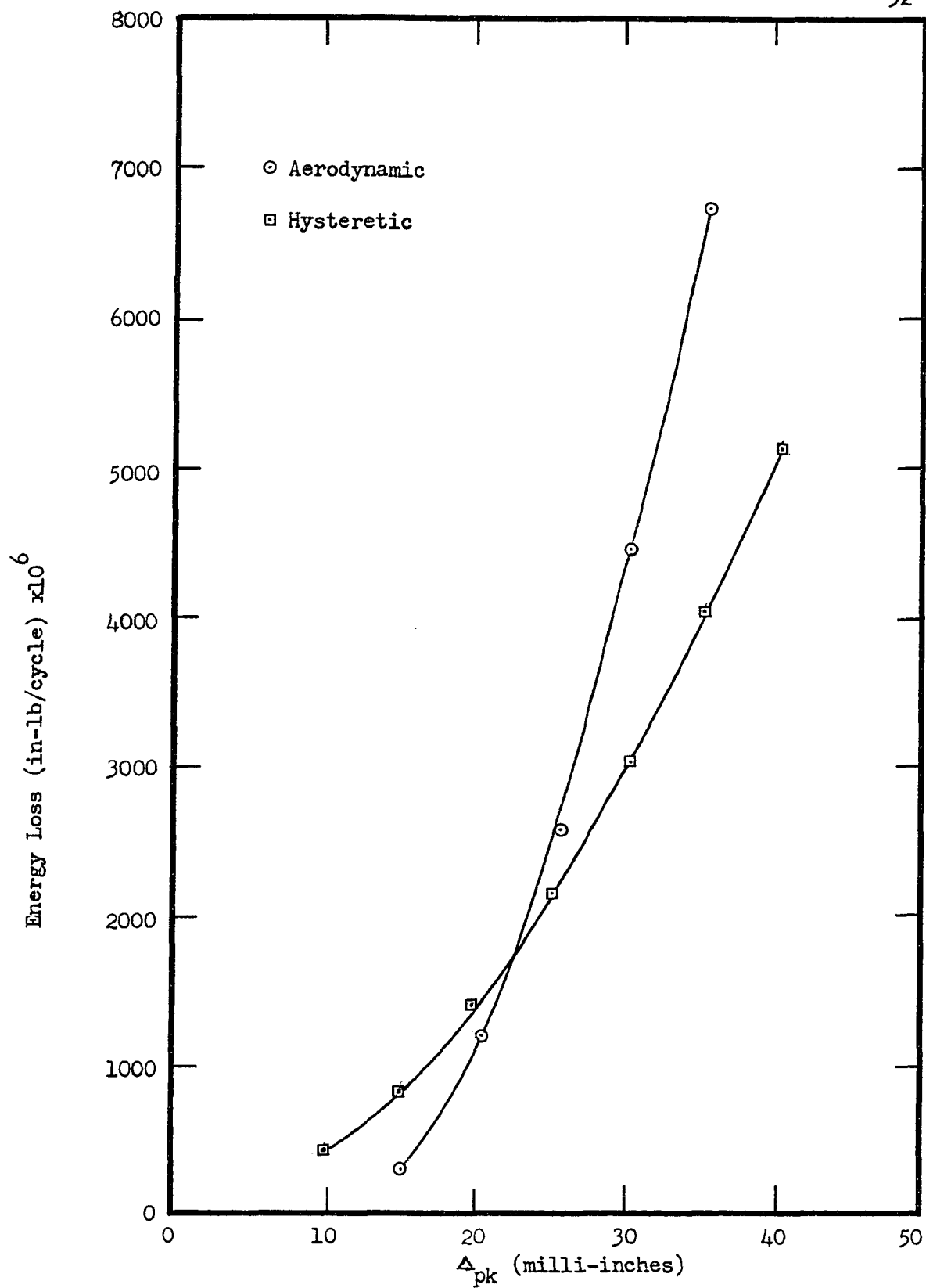


Fig. 19 Beam no. 4. Energy Loss against Tip Deflection

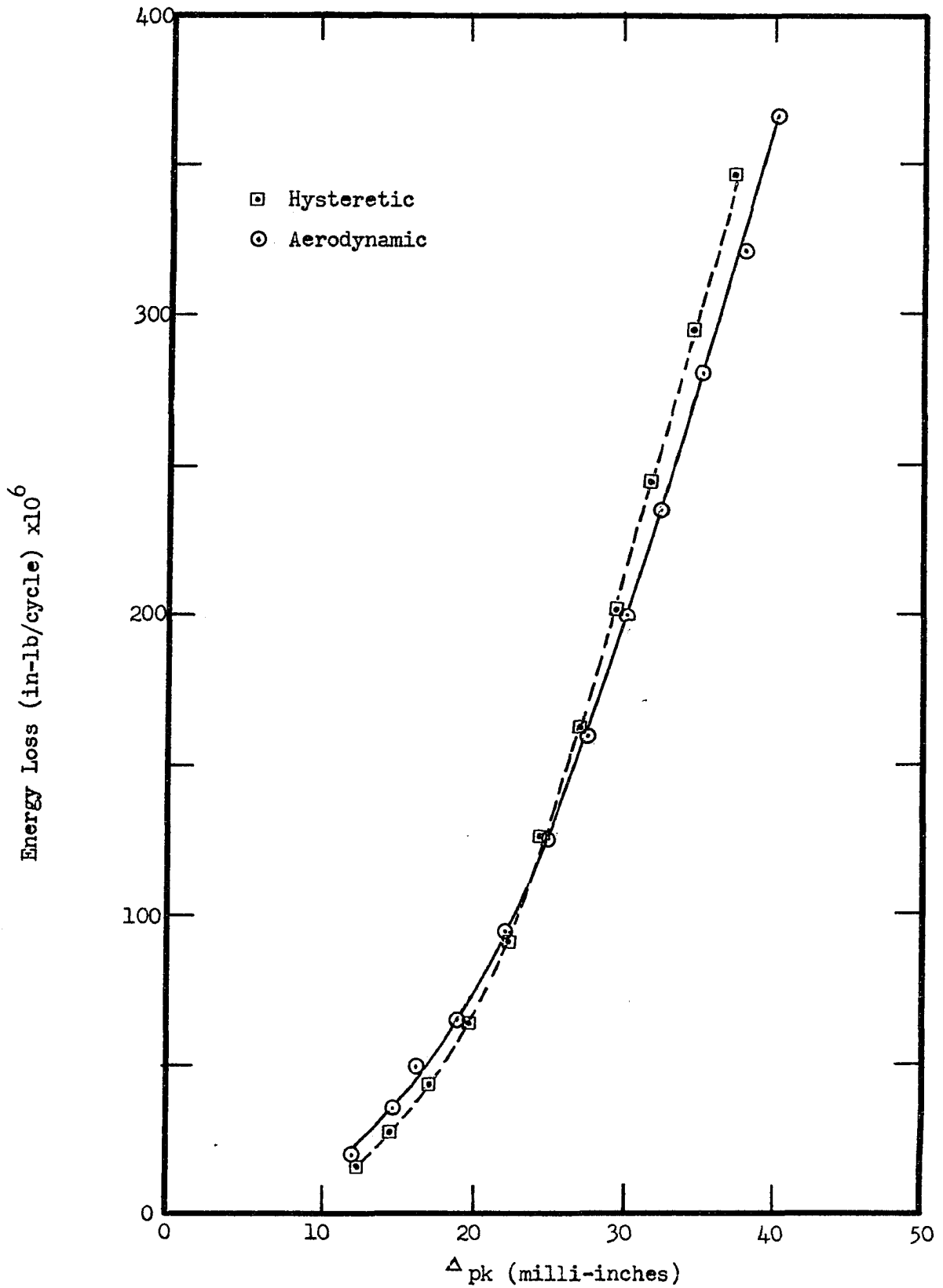


Fig. 20 Beam no. 5. Energy Loss against Tip Deflection

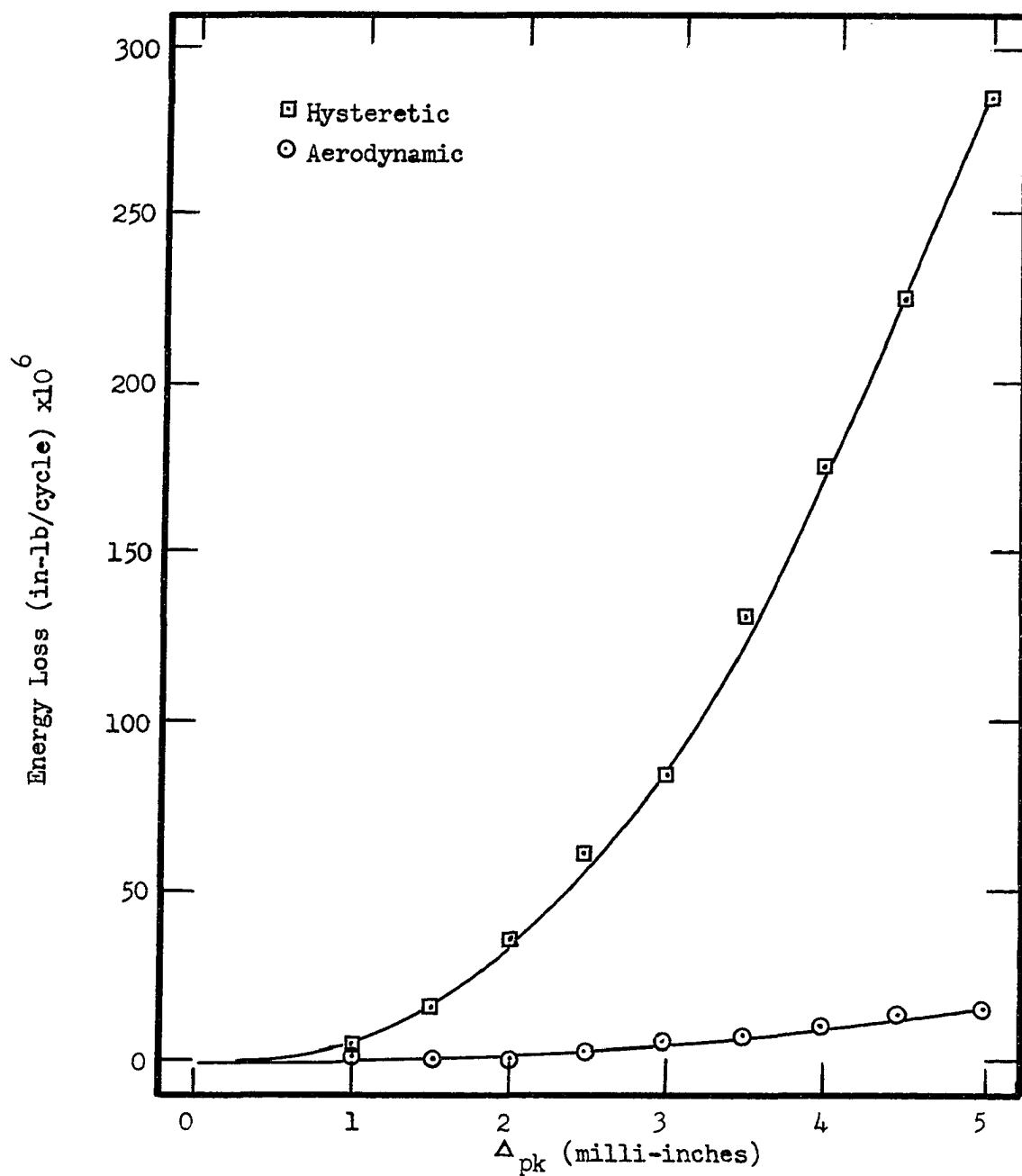


Fig. 21 Beam no. 6. Energy Loss against Tip Deflection

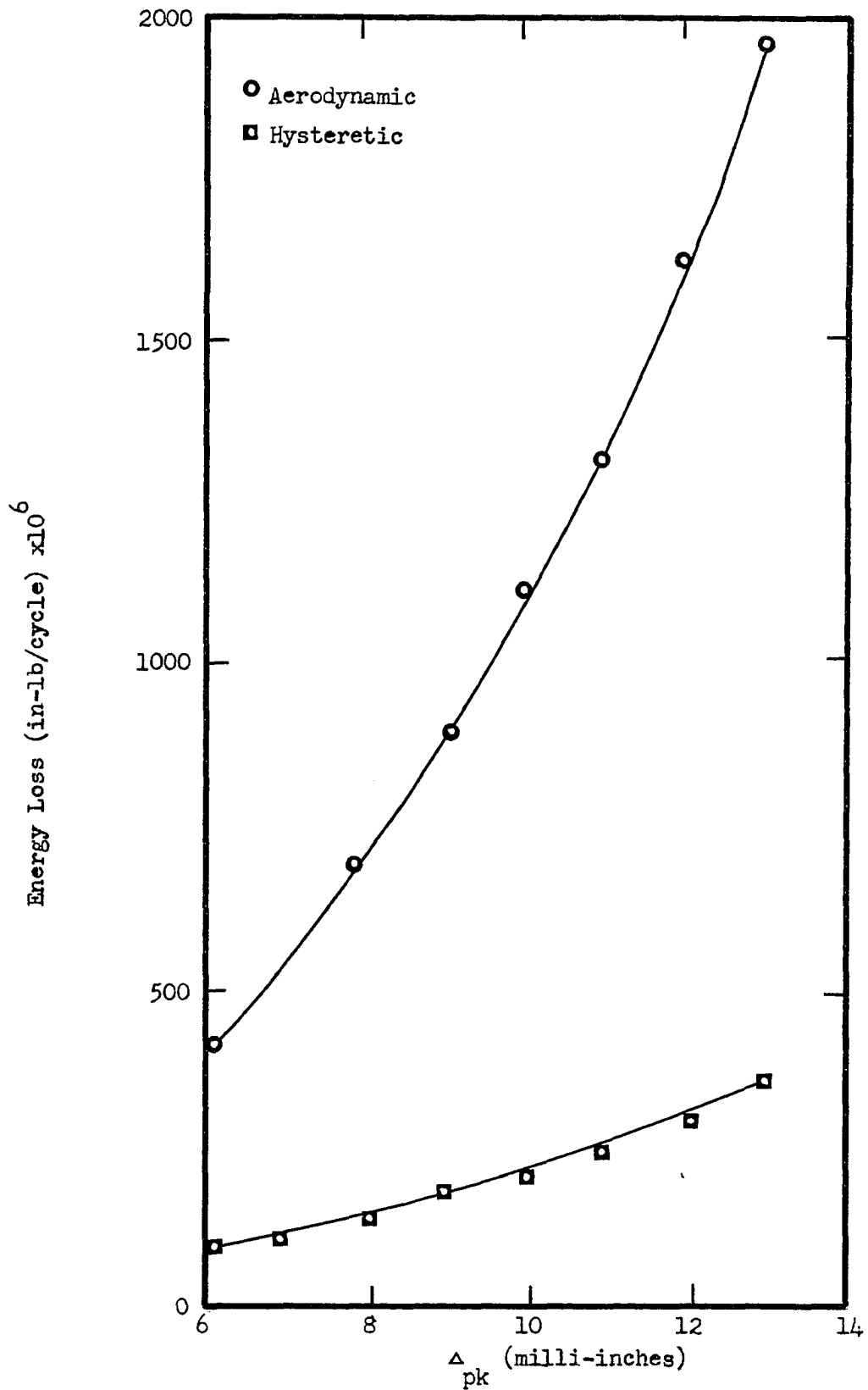


Fig. 22 Beam no. 7. Energy Loss against Tip Deflection

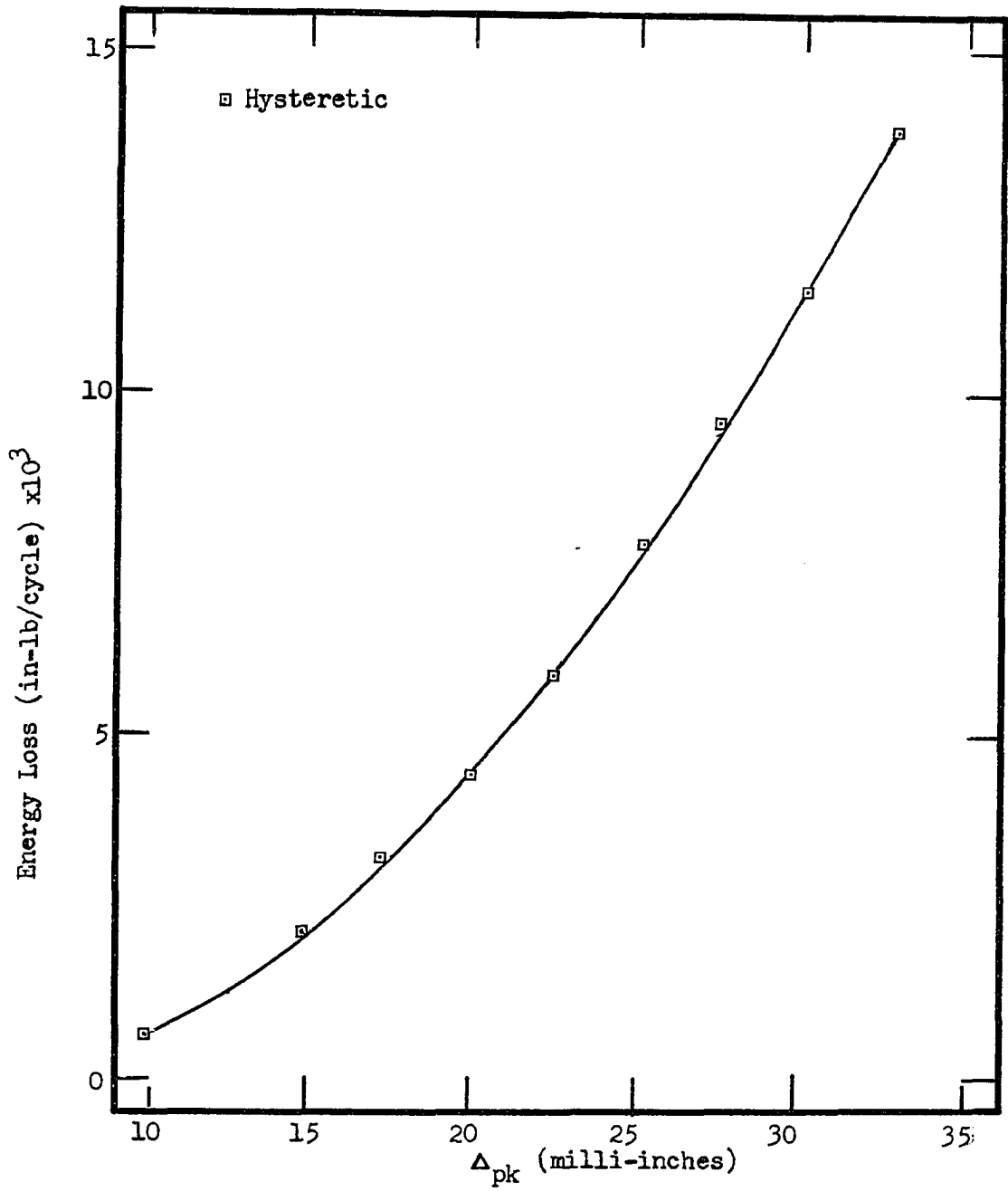


Fig. 23 Beam no. 8. Energy Loss against Tip Deflection

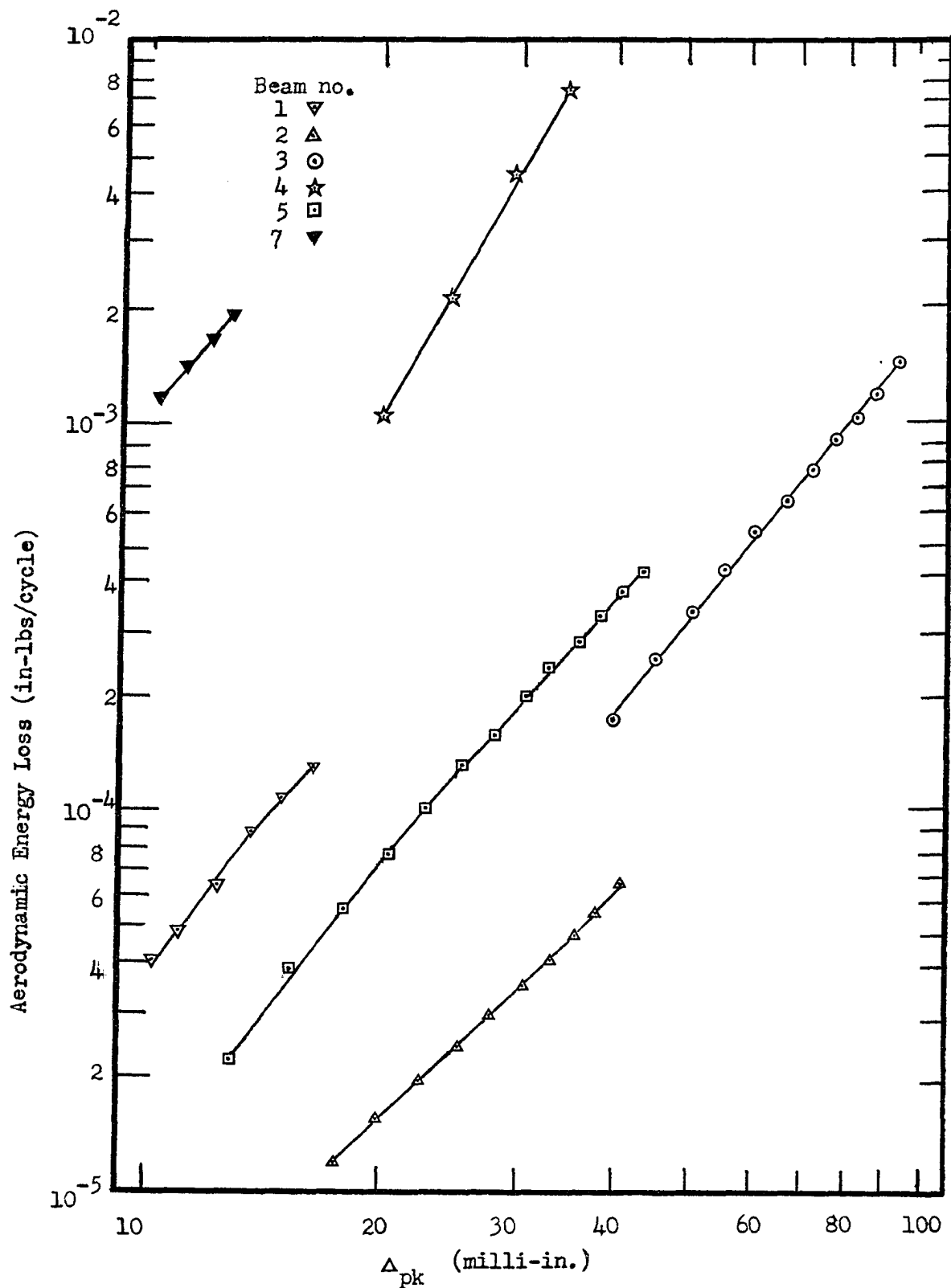


Fig. 24 Aerodynamic Energy Loss against Tip Deflection

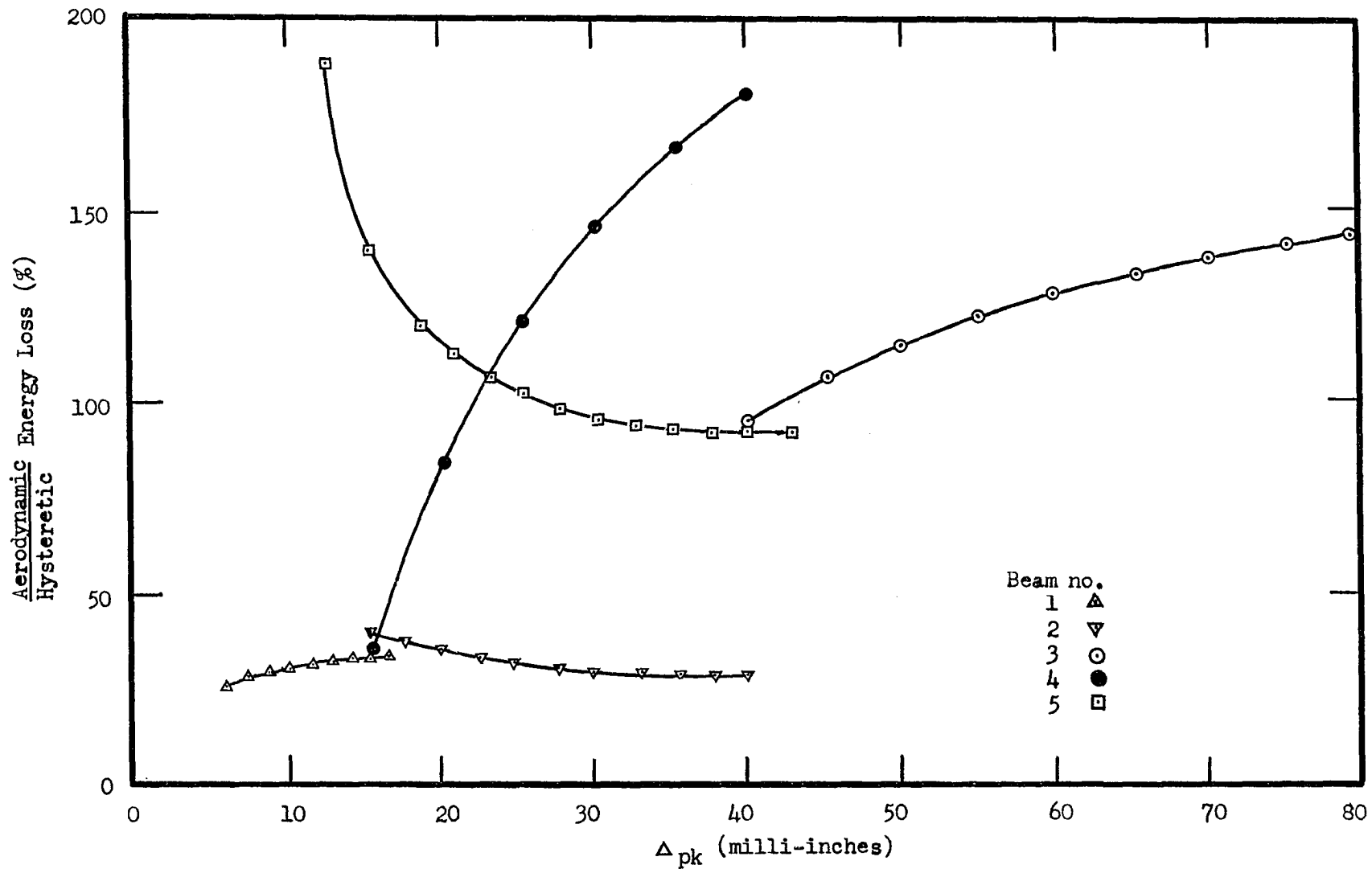


Fig. 25 Aerodynamic Hysteretic Energy Loss against Tip Deflection

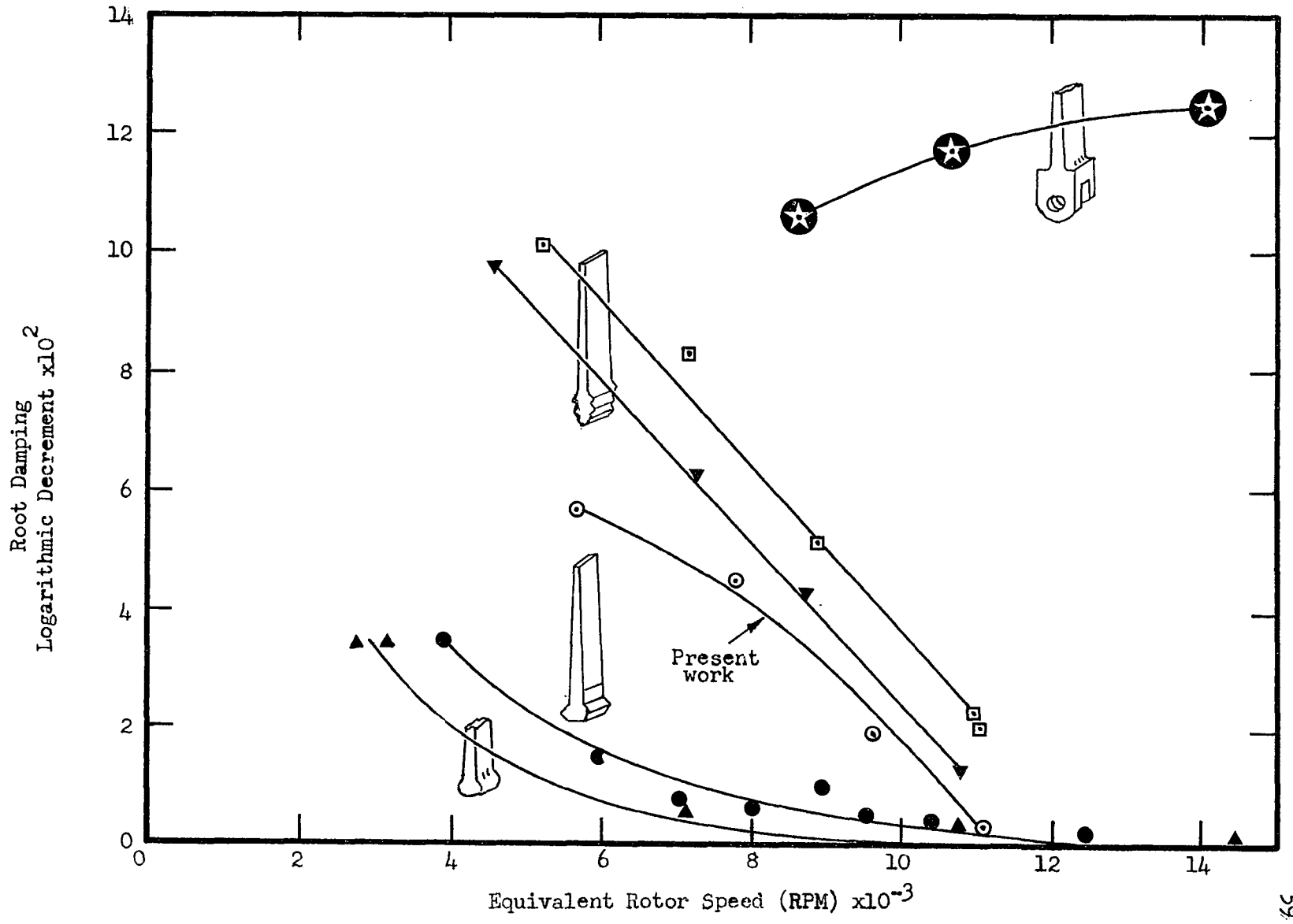


Fig. 26 Root Damping against Equivalent Rotor Speed

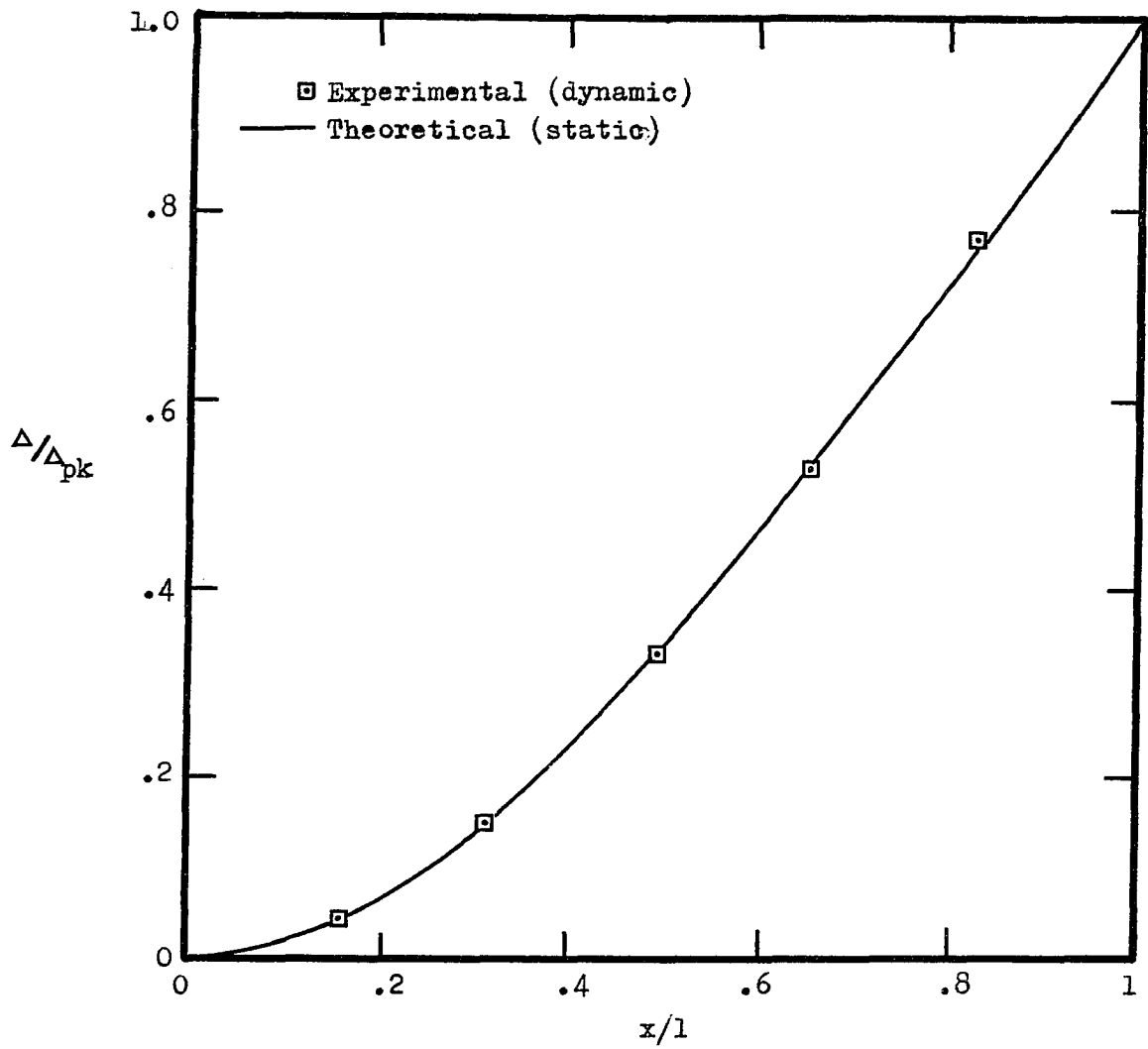


Fig. 27 Non-dimensional Beam Displacement Profile (Beam no. 4)

APPENDIX A

MATERIAL AND GEOMETRIC PROPERTIES OF THE BEAMS TESTED

BEAM NO.	1	2	3	4	5	6	7	8
MATERIAL	6061-T6 ALUMINUM	6061-T6 ALUMINUM	6061-T6 ALUMINUM	BRASS	BRASS	304 SS	304 SS	LOW CARBON STEEL
DIMENSIONS (inches)	$6 \times 1\frac{1}{2} \times \frac{1}{4}$	$6 \times 1\frac{1}{2} \times 0.1$	$11 \times 1.88 \times 0.1$	$6 \times 1 \times \frac{1}{4}$	$11 \times 1 \times \frac{1}{4}$	$6 \times 1\frac{1}{2} \times \frac{1}{4}$	$11 \times 1\frac{1}{2} \times \frac{1}{4}$	$6 \times 1\frac{1}{2} \times \frac{1}{4}$
1st NAT FREQ (THEOR) cps.	225	89	26.5	147	43	237	69.1	216
1st NAT FREQ (EX'L) cps.	216	88	26.1	127	37.0	202	67.1	202
n*	2.49	2.28	2.15	1.75	2.67	2.36	2.00	2.45
$J \times 10^{10}$ *	0.172	1.48	6.60	63.2	0.0406	0.354	5.05	0.0936
AERO. EXPONENT	2.50	2.00	2.53	3.26	2.40	-	2.60	-
$E \times 10^{-6}$ psi.	10.0	10.0	10.0	14.5	14.5	27.6	27.6	30.0
ρ_m lb/in ³	0.098	0.098	0.098	0.314	0.314	0.285	0.285	0.285

* Dimensions such that for $D = J\sigma^n$ with σ in psi., D is in in-lb/in³/cycle.

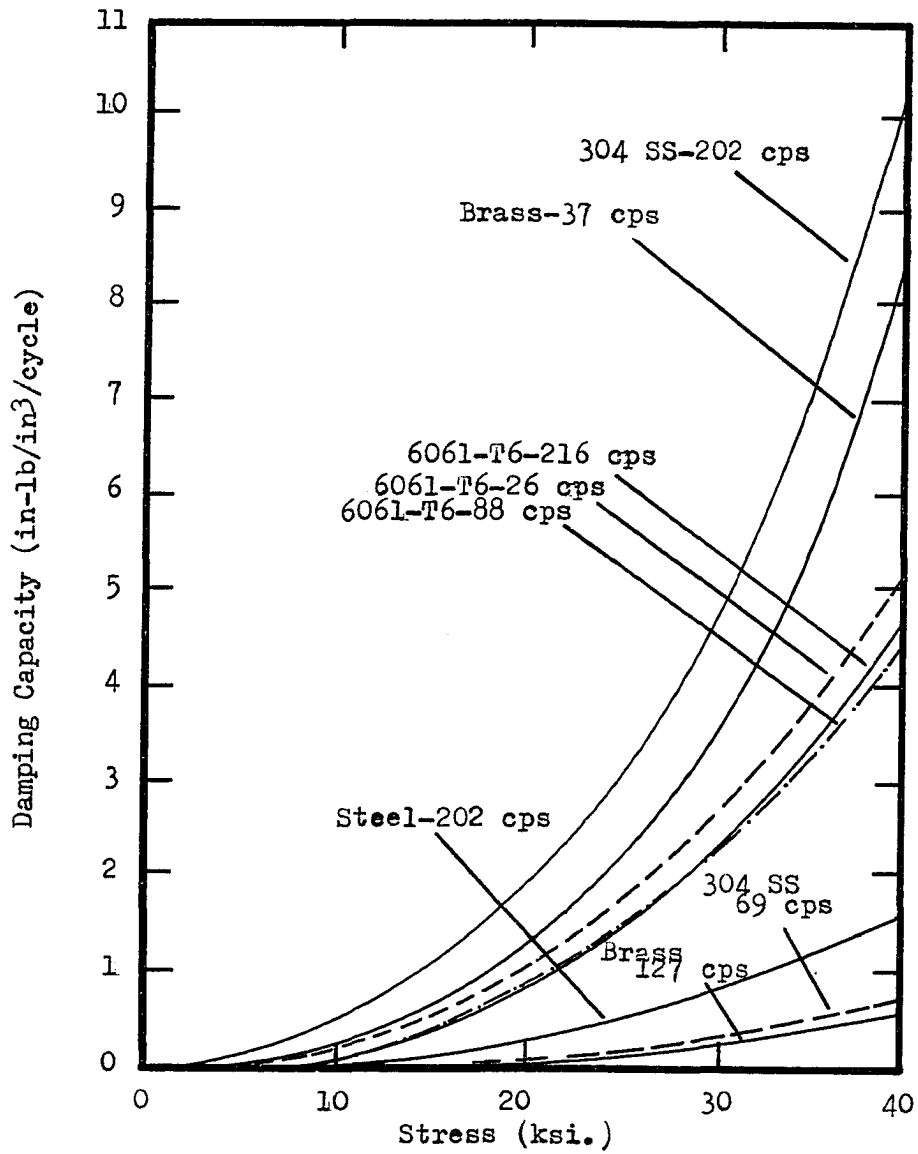


Fig. 28 Hysteretic Damping Capacity against Stress

APPENDIX B

VIBRATION MONITORING DEVICES USED

Three types of transducers were used to monitor vibrations: strain gages, accelerometers and a capacitive pickup.

Strain gages were of the metal foil type. Wherever possible, temperature compensated gages were used. Strain gage output was amplified in a carrier amplifier and recorded on a light beam recorder. (Appendix C)

Bruel and Kjaer piezoelectric accelerometers were used in all cases. Type 4333 accelerometers were used on the shaker table (figure 29) to monitor motion. Miniature accelerometers (0.07 oz.), type 4336, were used on test specimens for monitoring of motion. Accelerometer output was monitored on an oscilloscope or a frequency analyser (Appendix D).

A Bruel and Kjaer capacitive pickup, type MM004, was used for tracing nodal patterns. This transducer measures the capacitance change between itself and the specimen as the distance between the two varies due to vibration. The capacitive pickup yields only qualitative information about displacement.

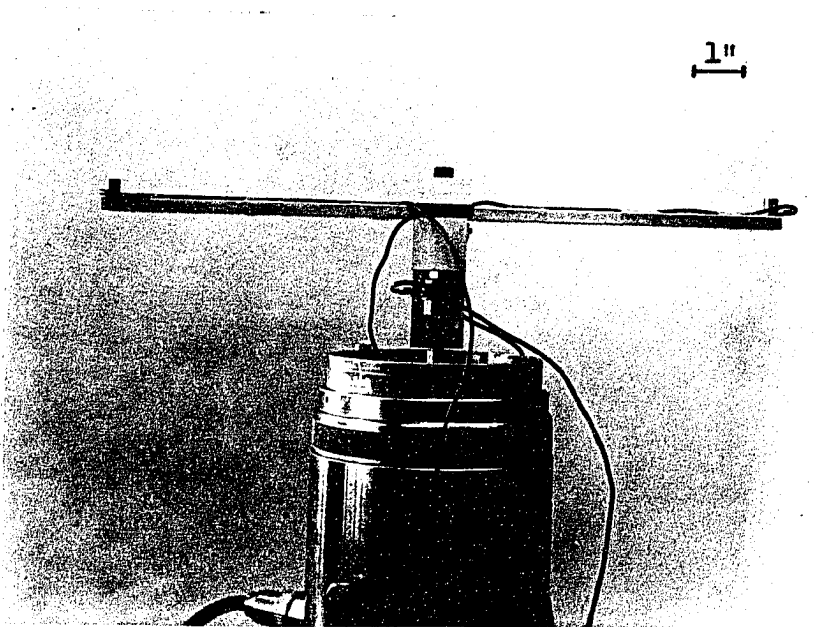


Fig. 29. Shaker Table

APPENDIX C

BLADE EFFECT TEST EQUIPMENT

Strain gages were selected for the natural decay tests since they were compatible with the light beam recorder system. This allowed recording of the full damped sinusoid motion on a six inch trace width, figure 30, with the chart speed ranges up to 2000 mm/sec.

Gages were connected to an SE Laboratories 4300/P Carrier Amplifier with a 4000 System Power Supply. Output was recorded on an S. E. Laboratories Model 2006 U. V. Recorder equipped with silicone-damped galvanometers. Frequency response of the entire system is flat within 3% to 400 cps at full trace width.

Figure 31 shows a block diagram of the test arrangement while figure 32 is an overall photograph. A close-up of the natural decay test rig is shown in figure 33 while the vacuum chamber is shown in figure 34.

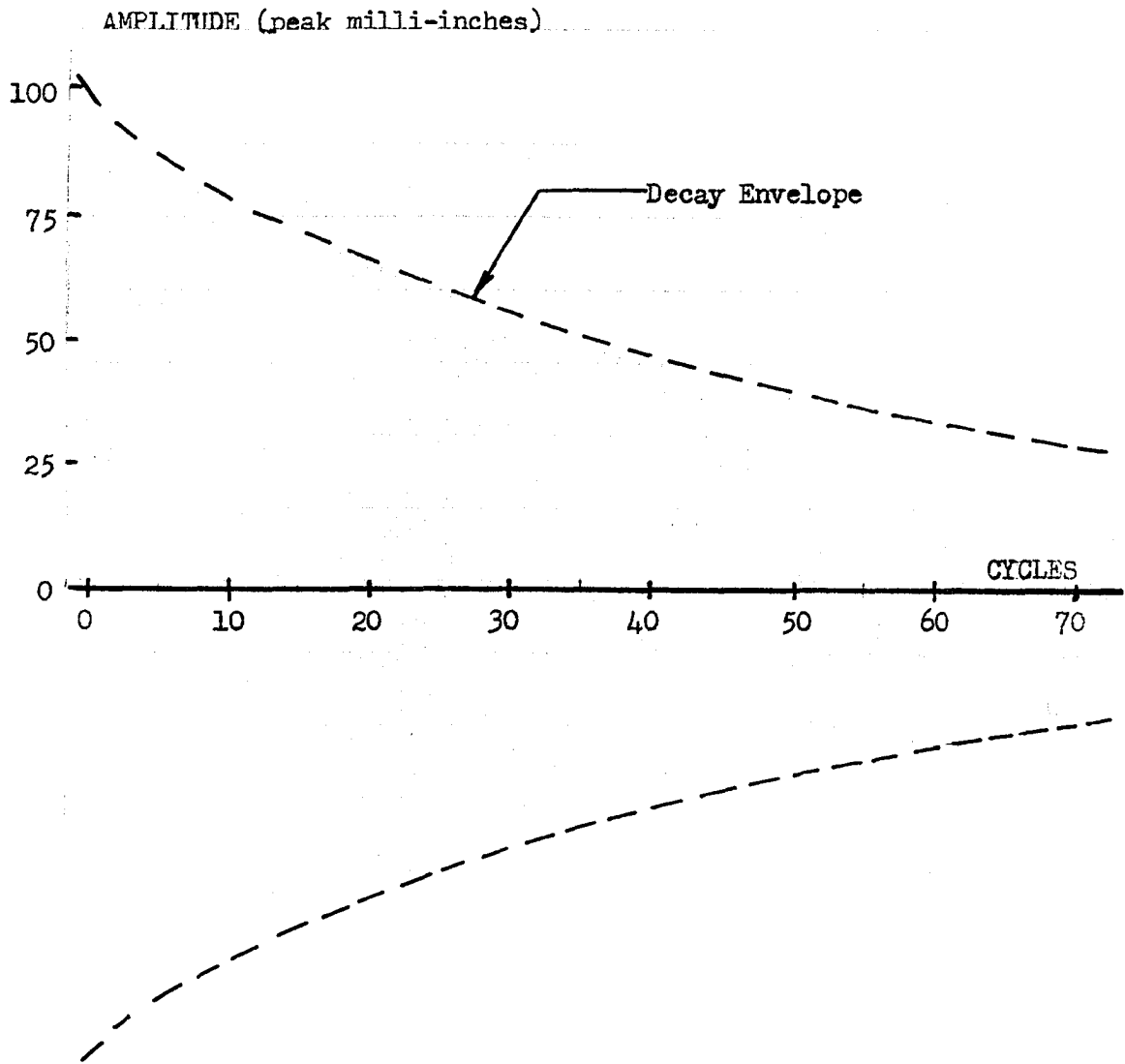


Fig. 30 Portion of a Typical Decay Curve from
the Light Beam Recorder

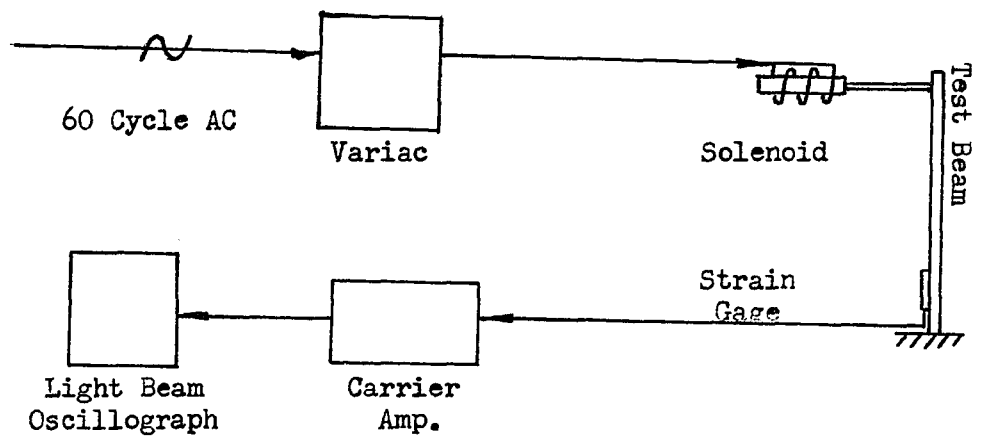


Fig. 31 Block Diagram of Natural Decay Test Apparatus

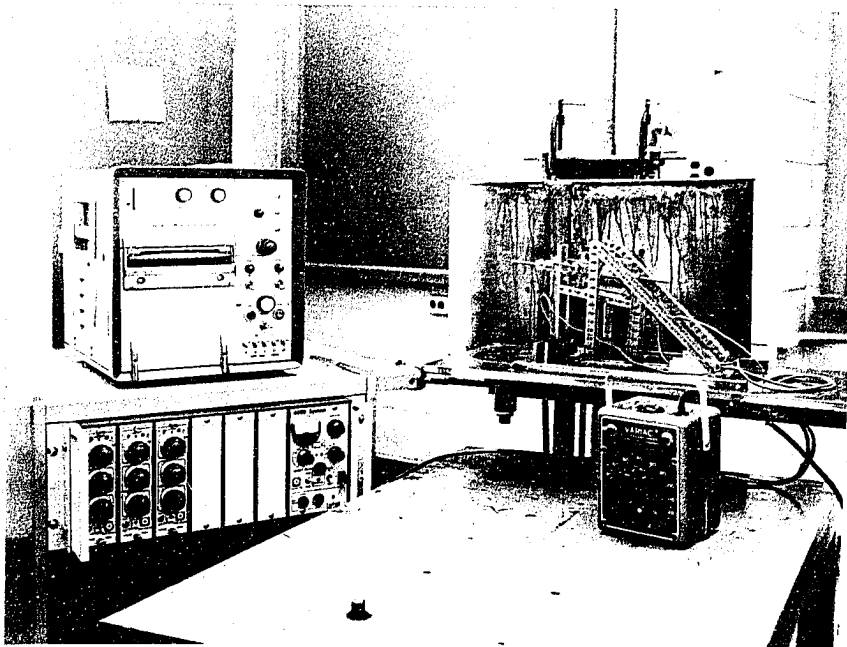


Fig. 32. Natural Decay Test Arrangement

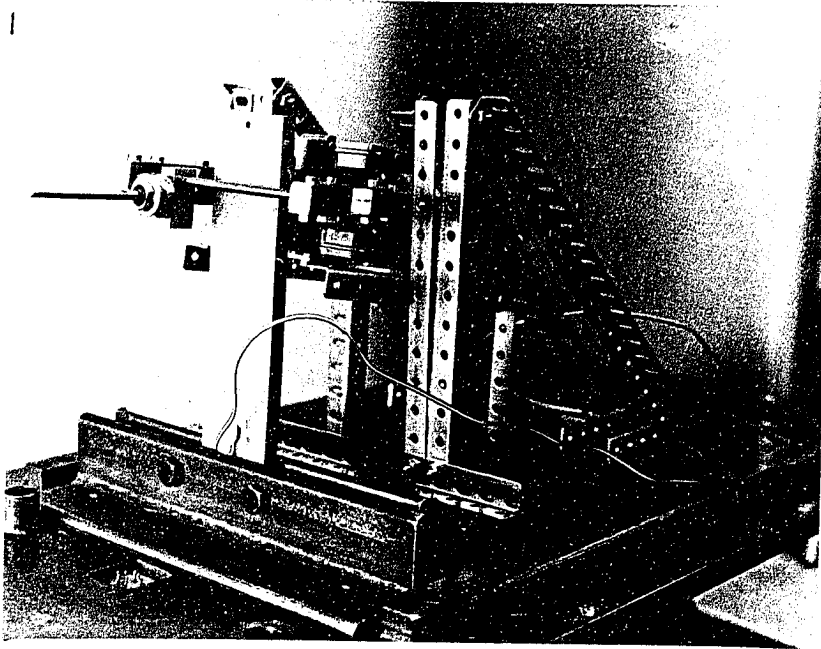


Fig. 33. Natural Decay Test Rig

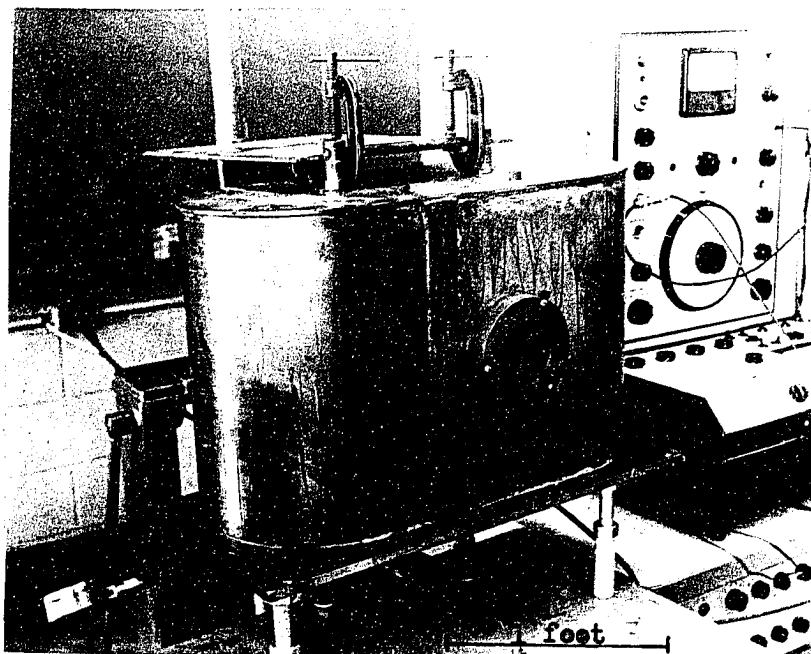


Fig. 34. Vacuum Chamber

APPENDIX D

FORCED VIBRATION SYSTEM

The forced vibration system was used for initial beam cycling, calibration of strain gage outputs (appendix F) and for forced vibration tests on root damping. A block diagram of the system is shown in figure 35, with a general view in figure 36. The signal generator generates a sinusoidal signal which may vary from 5 cps to 10 kcs. The signal is amplified in the power amplifier and sent to the moving coil of the electrodynamic shaker. The shaker has a stroke of ± 4 mm and a maximum force of approximately eight pounds. An accelerometer on the shaker table is used to feed back an acceleration signal from the shaker to the signal generator. This signal may be used to control table acceleration, displacement or velocity, as desired.

The output acceleration signal is fed to the analyzer which serves as both an amplifier and a continuous band-pass filter (from 6.3 cps to 6.3 kcs) to eliminate signal noise. The output signal may then be recorded on the strip-chart type level recorder. When it is desired to sweep a frequency range, the band-pass of the filter and the level recorder chart drive may be controlled from the signal generator for synchronous operation.

The Bruel and Kjaer Type 4336 accelerometers, when coupled to the Bruel and Kjaer frequency analyzer, Type 5011, have an accuracy of $\pm 2\%$ with frequency response flat within 2% from 2 cps to 25 kcs with stability better than 2% per year. Nominal accelerometer output is 4 mv/g.

A typical sweep of a resonant frequency as plotted on the level recorder is shown in figure 37.

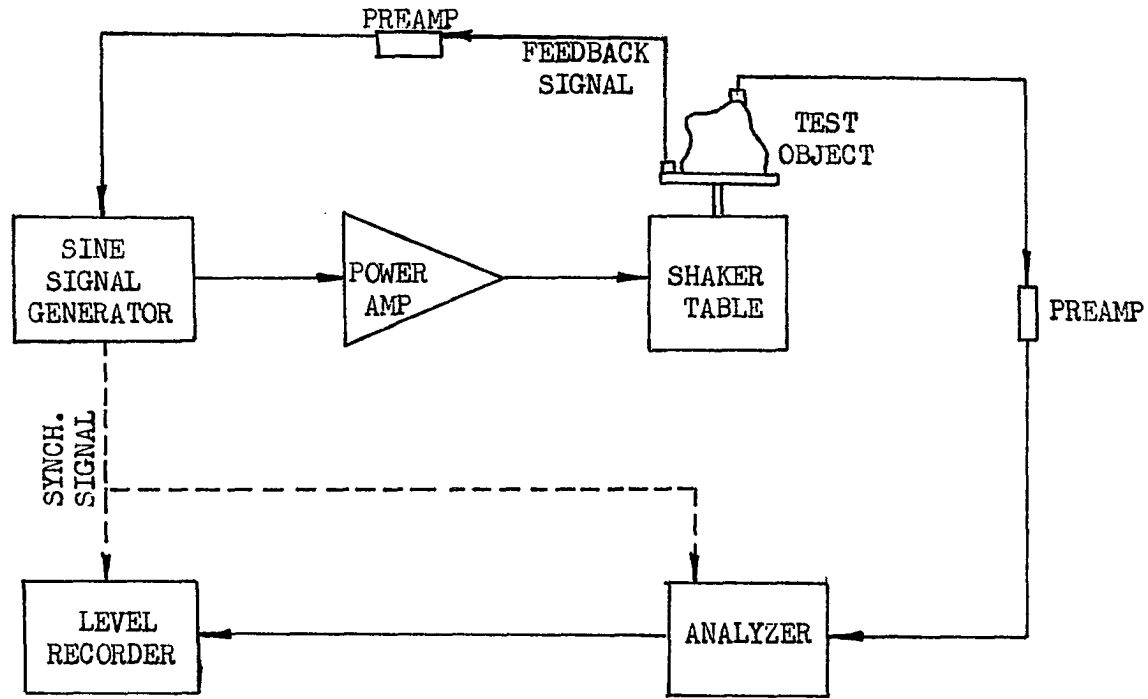


Fig. 35 Block Diagram of Forced Vibration Excitation Apparatus

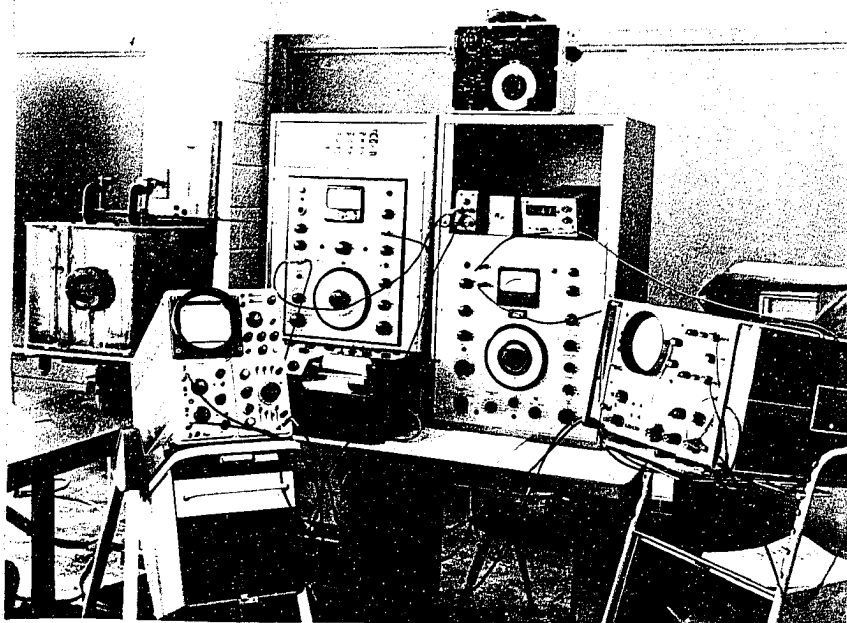


Fig. 36. General Laboratory Arrangement
Forced Vibration Tests

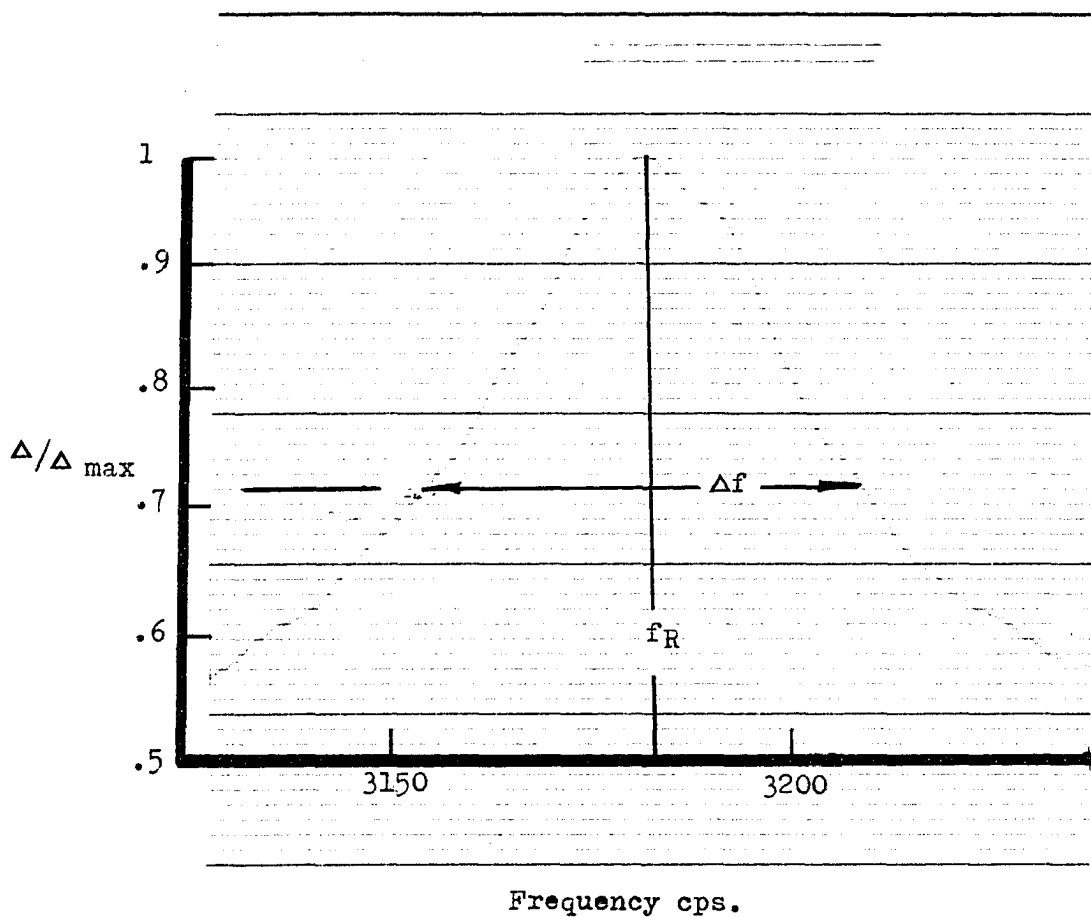


Fig. 37 Typical Level Recorder Output - Frequency against Amplitude

APPENDIX E

ROOT EFFECT TEST EQUIPMENT

The forced vibration system (appendix D) was used for root damping tests. The blade in question was hung from the appropriate disk and dead loads applied to simulate centrifugal forces. The shaker was attached to the blade with a pinned connection. Damping was monitored using the resonance bandwidth method. Frequency was measured on the digital counter and vibration was monitored by accelerometers on the exciter jig.

APPENDIX F

CALIBRATION OF STRAIN GAGE OUTPUT AGAINST BEAM TIP DEFLECTION

Since strain gages were used in the natural decay tests, it was necessary to calibrate the strain output against tip deflection. All strain gages were centrally located along the axis of the beam with the gage centre line one inch from the beam fixture. Beams were then bolted to the shaker table. A miniature accelerometer was fastened to the tip of the beam and the accelerometer cable was taped to prevent stray signals due to cable whip. No stray signals were found in the accelerometer output due to magnetic fields produced by the shaker table. When tests were run at high amplitudes, or with heavy beams, the beams were made symmetrical with respect to the shaker centre line, as shown in fig. 29, to prevent bending deflections in the shaft of the shaker.

The forced vibration system, as shown in figure 35, was then used to vibrate the beam in the first flexural frequency. The input power level was then varied and the strain gage output on the light-beam recorder was compared to the accelerometer output as read on the analyzer. Calibration was carried out up to the maximum tip deflection used in the natural decay tests. A typical calibration curve is shown in figure 38. Figure 38 also includes the theoretical strain as predicted from the static deflection curve of the beam subjected to a uniform load. The curve shows good agreement with this theory.

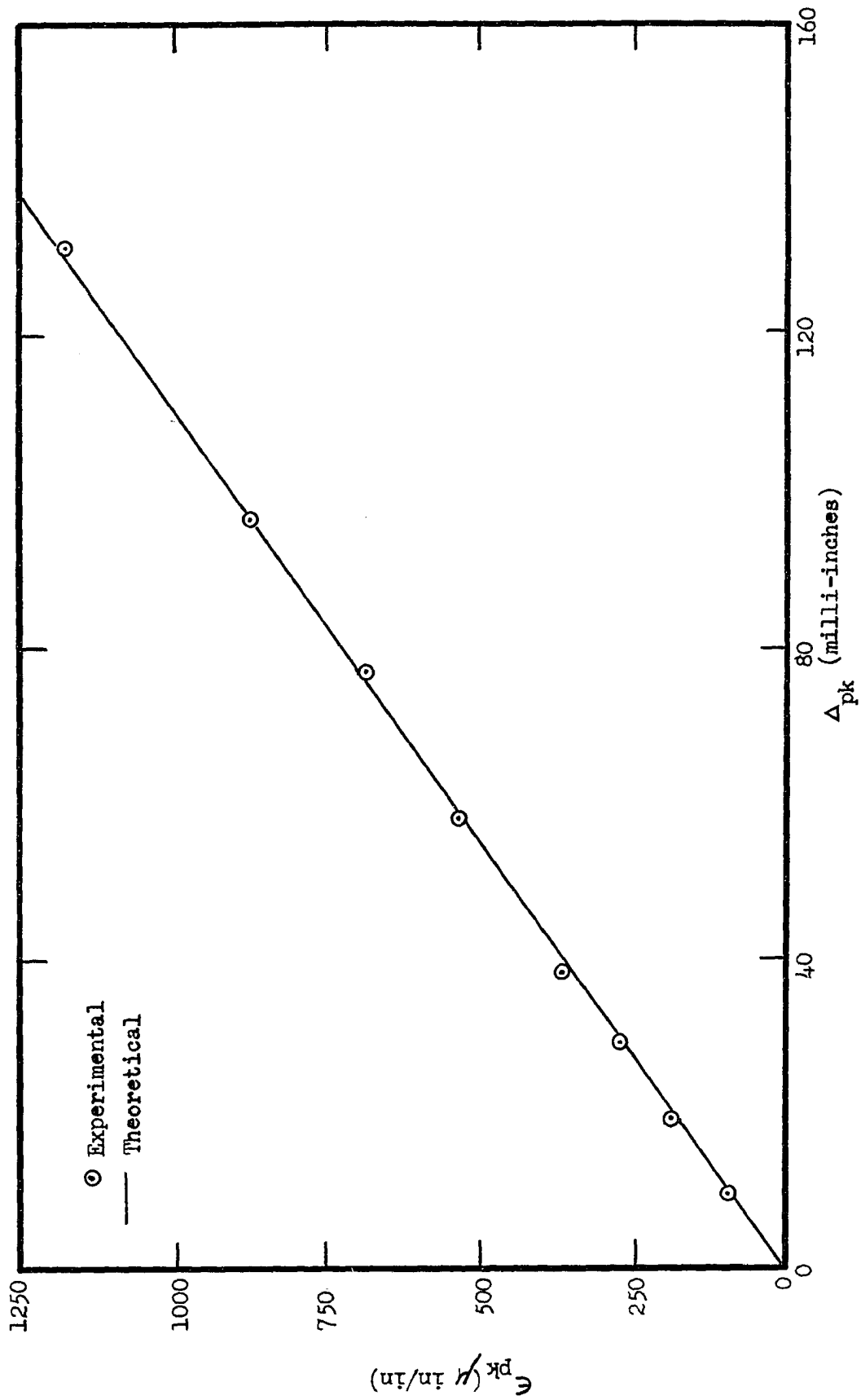


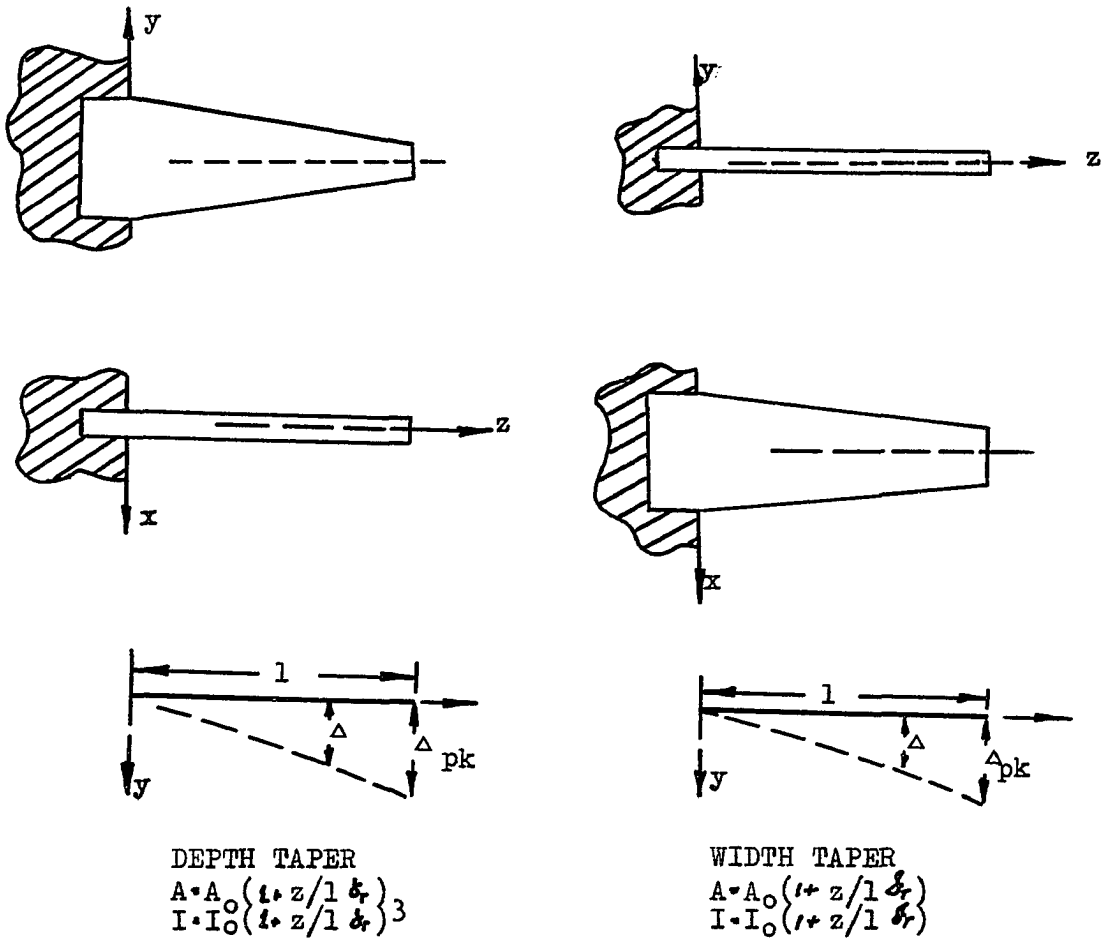
Fig. 38 Typical Calibration of Strain Gage Output against Tip Deflection (Beam no. 4)

APPENDIX G

EFFECTS OF TAPER ON HYSTERETIC DAMPING

Due to the complex shape of the turbine blade, it is difficult to analyze the effects of all geometric variables simultaneously. Thus, an analysis of the effects of linear taper only (figure 39) were studied theoretically. An element method was chosen and programmed for the IBM 360/40 computer.

Due to the dependance of hysteretic damping on frequency in the higher frequency ranges, only the first flexural frequency was studied, and Lord Rayleigh's energy method (31) was chosen. The beam stiffness matrix was determined, neglecting shear deflection and rotary inertia. The load (due to the beam's own weight) was applied and nodal deflections calculated. Rayleigh's method was then applied to determine the natural frequency. The nodal deflections were then non-dimensionalized with maximum tip amplitude. This non-dimensional displacement profile is shown in figure 40 for depth taper and figure 41 for width taper. Figure 40 also shows profiles calculated by Carnegie (31) from the solution of the Euler-Bernoulli equation for the beam, which he verified by experiment. Agreement between the two methods was found within 2%. A comparison of calculated beam natural frequencies as compared with those of Carnegie is given below. (based on a nominal beam similar to beam no. 4)



Where: A cross-sectional area

A_0 cross-sectional area at beam base

I moment of inertia

I_0 moment of inertia at beam base

δ_t taper coefficient

Fig. 39. Taper Nomenclature

DEPTH TAPER

δ_T	FREQUENCY (cps)	
	CALCULATED	REF. 31
+0.50	145	144
0	151	151
-0.25	156	156
-0.50	165	165

WIDTH TAPER

δ_T	FREQUENCY (cps)	
	CALCULATED	REF. 32
+1.00	118	120
+0.50	131	133
0	151	151
-0.50	186	185
-1.00	314	-

Excellent agreement is shown between the two methods in both frequency and deflection profile. Deflections were then used, in conjunction with element stiffness matrices to compute nodal stresses. The nodal stresses were then assumed uniform over the elemental and hysteretic energy dissipation summed from all elements. Results of hysteretic energy dissipation against tip amplitude are plotted in figure 42.

From figure 42 it may be seen that, for a fixed tip amplitude, width taper has little effect on energy dissipation. Depth taper has a more significant effect, since this affects moment of inertia to the third power. Thus, depth taper has a larger effect on stress than width taper. It may be seen from the curves that the case of negative taper, as is common in turbine blades, of either width or depth increases tip deflection required to dissipate a given amount of energy. Thus, the greater the negative taper of the blade, the larger the tip amplitude (and maximum stress) under a given excitation function. It may be noted that depth or thickness taper is far more critical in this respect, yet a blade of constant chord and radially outwards decreasing thickness is common.

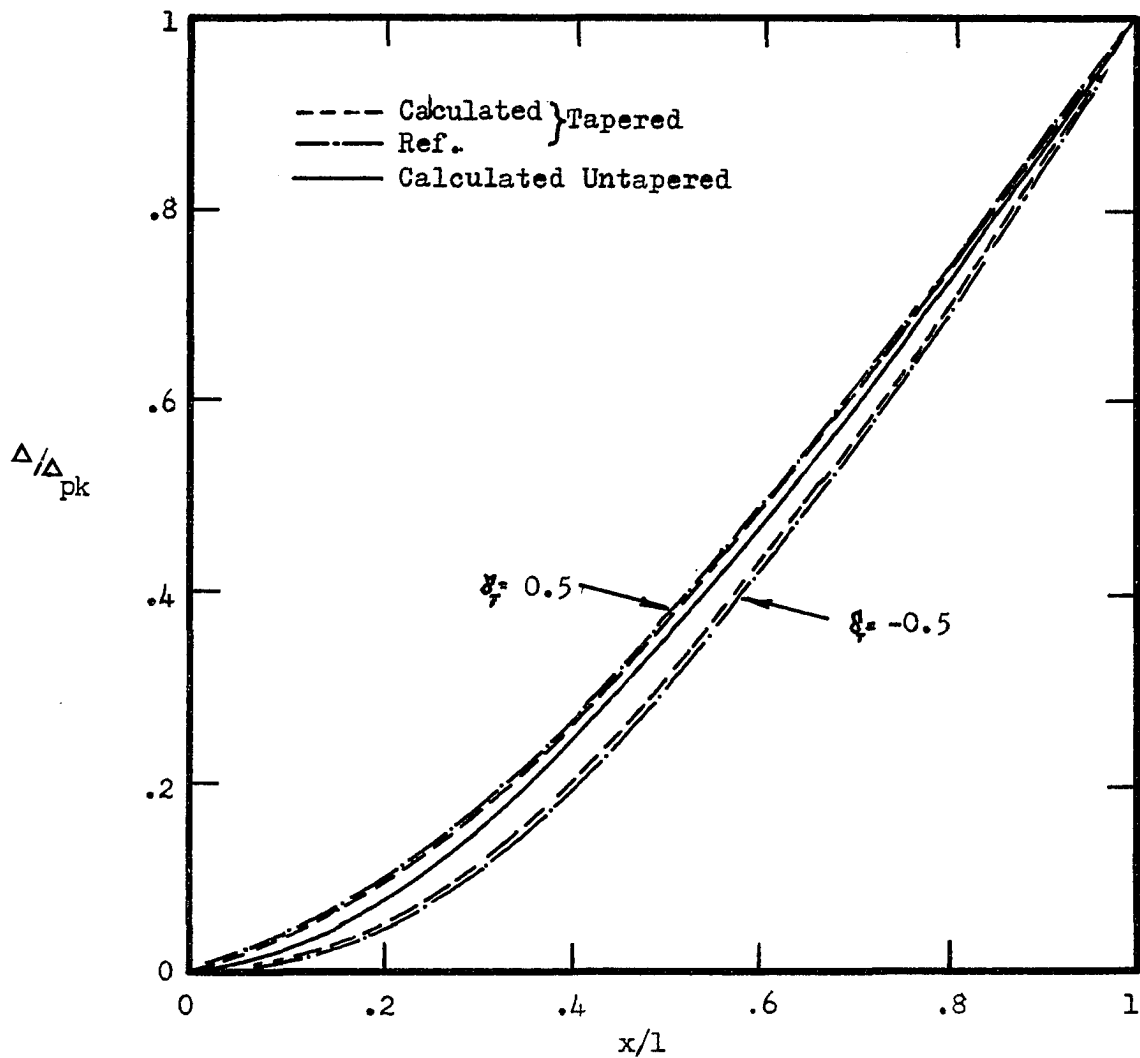


Fig. 40 Effect of Depth Taper on Beam Displacement Shape (First Flexural Mode)

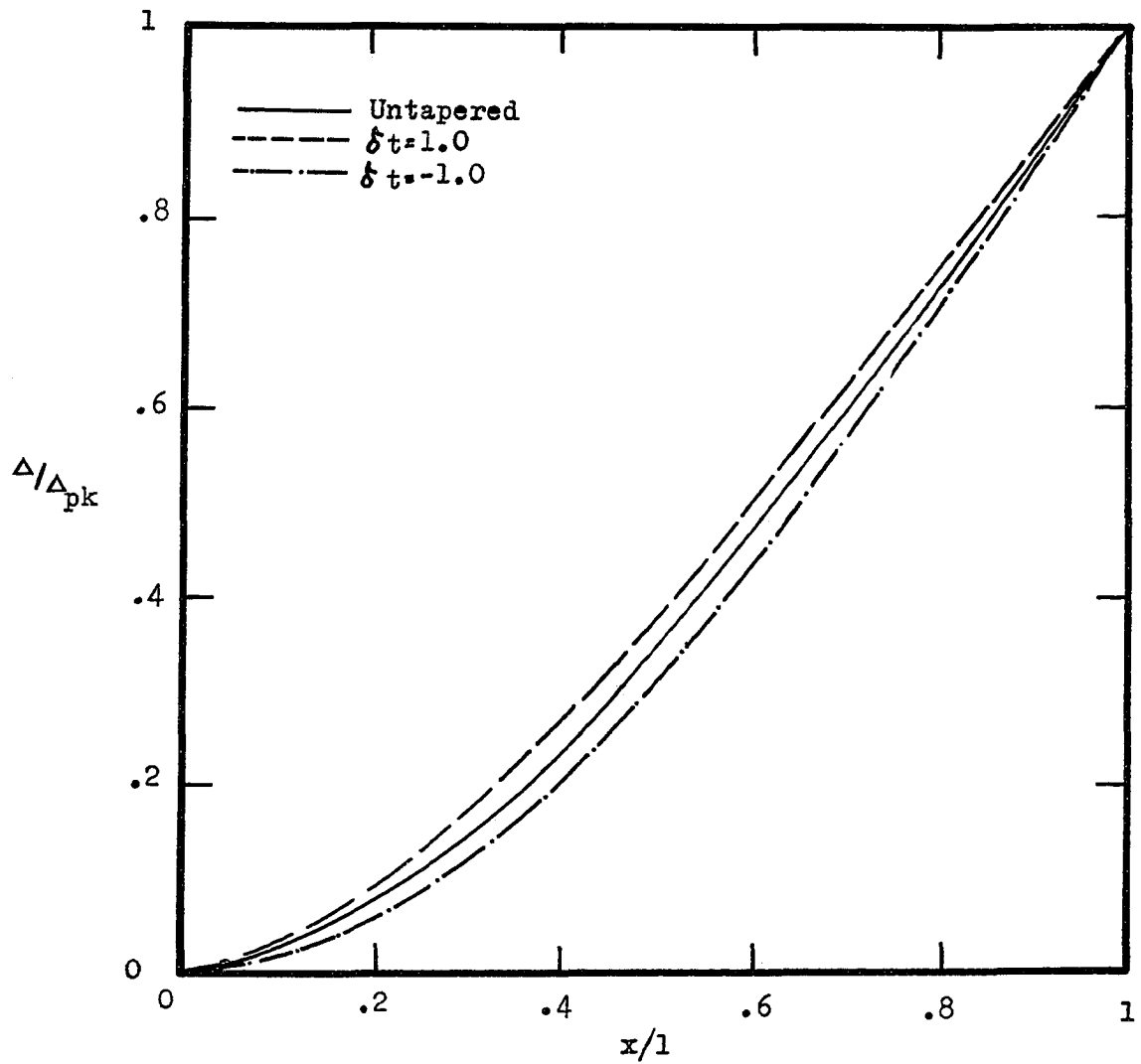


Fig. 41. Effect of Width Taper on Beam Displacement Shape (First Flexural Mode)

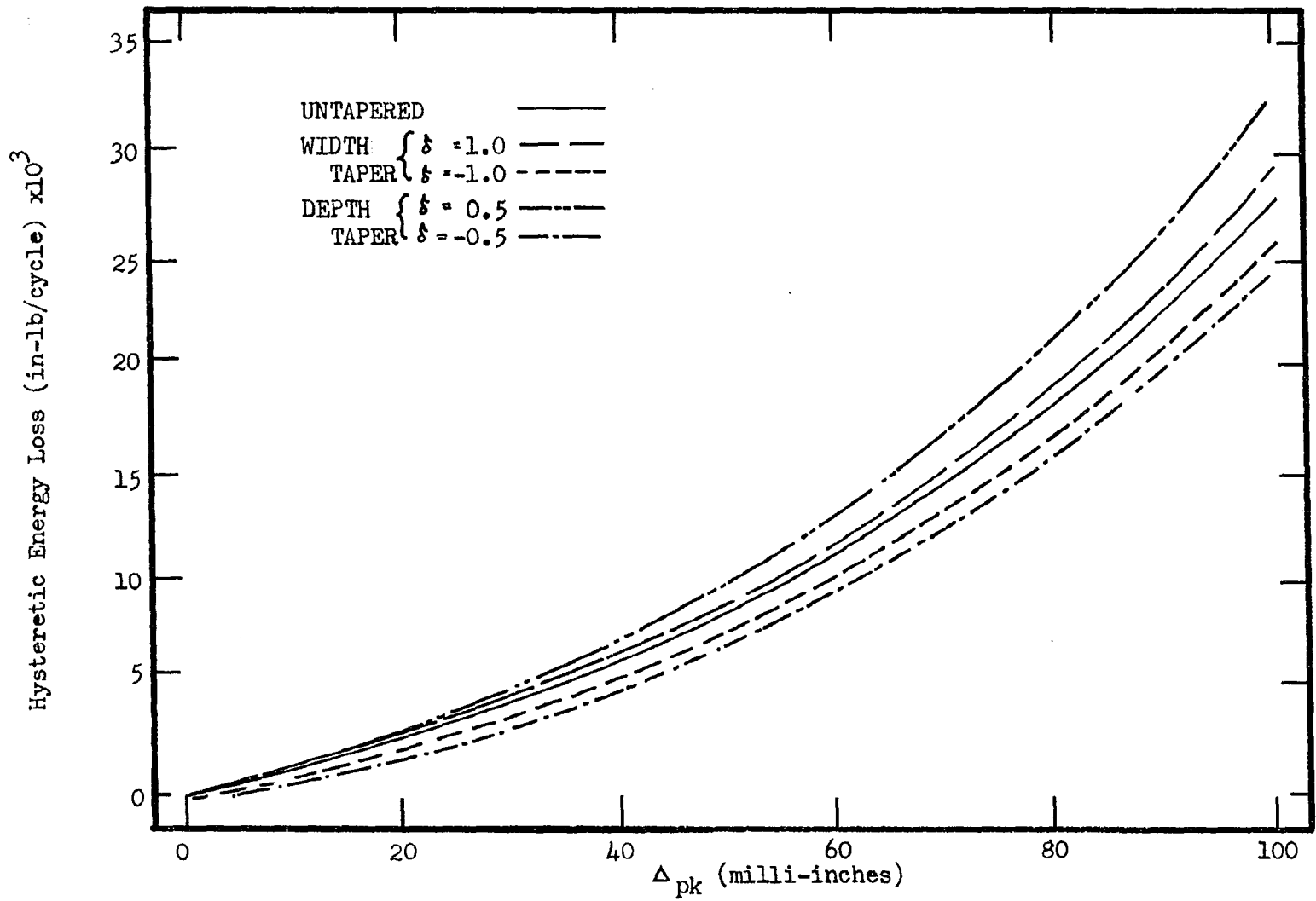


Fig. 42 Effect of Taper on Hysteretic Energy Dissipation against Tip Deflection for a 6"(1 1/2"x 1/4" Root) Brass Beam

AERODYNAMIC ENERGY LOSS IN MOVING AIR

Hanson, Meyer and Manson (22) suggest a correlation exists for energy loss in moving air considering both vortex and propulsive losses. They found

$$\delta_a = \frac{13.4}{R} \frac{V}{f_R c} \quad \text{for } 0.1 < \frac{V}{f_R c} < 1.0$$

$$R = \frac{\rho_m}{\rho_a} \frac{(0.229A_0 - 1.044A_t)}{c^2}$$

where

- δ_a log decrement due to aerodynamic damping
- V mean air velocity relative to blade
- f_R first natural frequency of blade (cps)
- c chord (inches)
- ρ_m material density
- ρ_a air density
- A_0 blade base cross section (in²)
- A_t blade tip cross section (in²)

Consider a typical case for beam no. 1

$$A_0 = A_t = 0.382 \text{ in.}^2$$

$$c = 1.50 \text{ in.}$$

$$\rho_m = 169 \text{ lbs./ft.}^3$$

$$f_R = 226 \text{ cps.}$$

Typically in a prototype engine

$$V = 500 \text{ ft./sec.}$$

$$\rho_a^{-1} = 12.5 \text{ ft.}^3/\text{lb.}$$

then

$$R = 465$$

$$\delta_a = 4.25 \times 10^{-2}$$

Consider the approximation of equation (A)

$$\delta = \frac{\Delta U}{2U}$$

For $\Delta_{pk} = 10 \times 10^{-3}$ in.

$$U = \frac{2Ebh^3}{1^3} \Delta_{pk}^2$$

$$= 1.45 \times 10^{-2} \text{ in.-lb.}$$

Then, due to aerodynamic damping in moving air

$$\Delta U = 2U\delta_a$$

$$= 1.23 \times 10^{-3} \text{ in.-lb./cycle}$$

In still air at this tip deflection the aerodynamic energy loss per cycle was determined experimentally to be 4.0×10^{-5} in.-lb./cycle.

This calculation indicates that aerodynamic damping in moving air may be thirty times the value in still air. Thus it is probable that in an engine operating under design conditions, aerodynamic damping due to moving air may be far greater than any other form of energy dissipation.

However, energy dissipated decreases as frequency increases. Also, aerodynamic energy dissipation decreases as deflection decreases. Thus, at modes higher than the first flexural, the energy dissipation to the air will decrease and may become insignificant with respect to material hysteretic damping at higher and complex modes.

APPENDIX I

THE COMMERCIAL EQUIPMENT USED

1. Bruel and Kjaer Automatic Vibration Exciter Control Type 1025
2. Philips Excitation Amplifier GM 5535
3. Philips Electrodynamic Vibration Exciter model PR 9270/01
4. Bruel and Kjaer Accelerometer Preamplifier Type 2622
5. Bruel and Kjaer Two Channel Power Supply Type 2803
6. Bruel and Kjaer Frequency Analyzer Type 5011
7. Bruel and Kjaer Level Recorder Type 2305
8. Monsanto Digital Counter-Timer Model 100A
9. S. E. Laboratories U. V. Recorder 2006
10. S. E. 4000 Amplifier System with Type 4300/P Carrier Amplifiers
11. Bruel and Kjaer Accelerometers Type 4333 and Type 4336
12. Bruel and Kjaer Accelerometer Preamplifier Type 2623
13. Bruel and Kjaer Capacitive Transducer Type MM 004
14. Bruel and Kjaer Cathode Follower Type 2615
15. Hewlett-Packard Oscilloscope Model 175 A with 1750 B Dual Trace
Vertical Amplifier
16. Tektronix Type 564 Storage Oscilloscope with 3A1 Dual Trace
Amplifier and 3B3 Time Base

VITA

1945 Born in Windsor, Ontario, Canada.

1967 Received the degree of Bachelor of Applied Science in Mechanical Engineering from the University of Windsor, Windsor, Ontario.

1969 Presently a candidate for the degree of Master of Applied Science in Mechanical Engineering at the University of Windsor.